A Technique for Two-Dimensional Photoelectronic Astronomical Imaging, With an Application to Lunar Spectral Reflectivity Studies

by

Jay Stuart Kunin

Submitted in
Partial Fulfillment
of the Requirements for the
Degree of Master of Science

at the

Massachusetts Institute of
Technology

September, 1972

Department of Earth and Planetary Sciences, July 17, 1972

Certified by: ______________

Accepted by: ______________

Chairman, Departmental Committee on Graduate Students

A Technique for Two-Dimensional Photoelectronic Astronomical Imaging,

With an Application to Lunar Spectral Reflectivity Studies

by
Jay Stuart Kunin

Submitted to the Department of Earth and Planetary Sciences, July, 1972, in partial fulfillment of the requirements for the degree of Master of Science

ABSTRACT

An improved silicon vidicon photometer system, based upon the prototype by McCord and Westphal (1972a) was designed and constructed. An observing program was planned and carried out to test the system, and extensive software development was undertaken to handle the data. The Apollo 17 landing site and neighboring areas of the lunar surface were investigated at four wavelengths in the visible and near infrared. Data are presented and discussed. Suggestions for further development of the system and further applications to lunar reflectivity are presented.

Thesis Supervisor: Thomas B. McCord
Title: Associate Professor of Planetary Physics

A C K N O W L E D G E M E N T S

The development of a modern astronicaml data system is a project of such complexity that it cannot be done with reasonable efficiency by one person. Thus this thesis, which is a report on one phase of the development of such a system, is in effect a project report. The author was directly involved in every stage of the project, and served as project director. However, several people deserve credit for their contributions to specific parts of the development effort: Mr. George Silvis of the M.I.T. Planetary Astronomy Laboratory (MITPAL) did a great deal of work on the mechanical design and fabrication of the camera head. Mr. John Luzwick of M.I.T. Lincoln Laboratory provided valuable engineering assistance. Mr. Paul Kinnucan of MITPAL was of great help in the development of the data processing system. Finally, a particular debt is due Mr. Jeff Bosel of MITPAL, whose electronics skill and trouble shooting ability were as valuable as his strong back.

The pictures used in this thesis were produced by the Jet Propulsion Laboratory, California Institute of Technology, through the courtesy of Dr. A. F. H. Goetz and Mr. John Morecroft.

I would like to thank Professor James A. Westphal of the California Institute of Technology, and my advisor, Professor Thomas B. McCord, for encouraging me to become involved with the vidicon system at one of its earliest stages; it has been a very interesting and educational association. In particular, Professor McCord served not only as advisor to me and to the project, but also as a dedicated participant in many stages of the project.

My wife Marty provided the requisite moral support; in addition, her ability to type from my handwriting is probably unique, as well as invaluable.

The author was supported by a Sloan Research Traineeship during this project. The cost of the project was borne by National Science Foundation Grant GP-31516.

TABLE OF CONTENTS

Chapter I -- Introduction

Many problems of interest in astronomy involve observations of extended sources; examples include galaxies, nebulae, and star clusters, as well as the sun, the moon, and the planets. Photography has been the standard method of recording astronomical images since it replaced hand drawing over a century ago. It has recently been shown, however, (McCord and Westphal 1972b) that a silicon diode array (SID) vidicon tube can be used as a replacement for the photographic process in a variety of astronomical applications. This project is a continuation of the development of this technique into a useful and efficient astronomical tool.

Although photography has been an effective recording technique, it suffers many disadvantages in some types of astronomical work. In particular, photometry using photographs is a difficult task. It is necessary to know both the gamma curve and the spectral response of the process, and to make use of instruments such as microdensitometers in order to determine the exact light level recorded on the plate or film. Comparing two or more pictures is often a difficult task. In addition, the time between the recording of an image and when it has been processed in order to view it is sometimes quite long. This can cut observing efficiency significantly.

There are obviously many advantages to using an electronic image recording system in place of a photographic one. The development of the SID tube (Crowell and Labuda, 1971) made possible the design and construction of a potentially very accurate and flexible two-dimensional photometry system. McCord and Westphal (1972b) showed that by cooling the tube, exposures of several hours are possible; combined with the tube's linearity, dynamic range, spectral response, and compactness, this makes for a usable two-dimensional photometer.

Based on the developers' and the author's experience with the prototype system, it was decided to carry out a project to further test the efficacy of the vidicon photometer. The first step was to redesign the system, particularly in those areas which were most inefficient. In addition, observing procedures were refined in conjunction with the operational improvements in the system. These areas are discussed in detail in Chapter II.

In order to handle the large number of pictures expected from the system -- more than 100 a night is not unusual -- a data processing system had to be developed. A major part of the project was devoted to making this system as simple to use as possible, while retaining the flexibility needed to accommodate a new data-gathering system. The data processing is detailed in Chapter III.

Finally, an observing program was planned and carried out as a test of the hardware and software. For this purpose, the spectral reflectivity of a portion of the lunar surface was chosen as a typical problem. It has been shown over the past several years that there are small (<10%) but significant differences in the spectral reflectance (color) curves of different areas of the moon (see McCord, et al., 1972) for a review of such work), and that these differences can be related to differences in mineralogy (Adams and McCord, 1970, 1971).

However, because of the nature of current photoelectric photometry, these data have to be gathered at one point at a time, the size of such a "point" varying from five to twenty km depending on telescope size, aperture size, and seeing conditions. It would therefore be extremely useful to be able to obtain data of this type over a two-dimensional area, both to determine large-scale reflectivity differences and to pinpoint areas which require further study. This type of study has been done by photographic and photoelectric methods; McCord (1968) extensively reviewed studies through 1967 and Soderblom (1970) used photoelectric photometry to map color differences. In addition, Apollo multi-spectral photography has provided some large-scale color information (Goetz, et al., 1971). The vidicon photometer data, on the other hand, are produced as picture element (pixel) numbers immediately upon readout; photographs are not used directly in the data processing, but only as a display during several of the steps, or as one form of final data presentation.

Chapter II -- The System

An RCA 4532A vidicon tube was used as the sensor. The quantum efficiency of the target (fig 1) ranges from a peak of 80% at $\lambda = .55\mu$ to 6% at $\lambda = 1.1\mu$, the longest wave length normally used in the system. Response in the near ultraviolet falls off primarily because of the anti-reflection coating on the target. The manufacturer's curve of MTF is reproduced in fig. 2. The particular tube used had no defects in the target large enough to cause visible effects.

The system used for this project was based on the prototype system mentioned above which has been fully described in the literature (McCord and Westphal, 1972b). Briefly, the prototype consisted of a simple dry-ice container, in which the tube and focus/deflection coil assembly were cooled, a mechanical shutter and a manually-rotatable filter wheel for basic photometry, electronics for controlling electron beam scanning and digitization and recording of data, and a cable connecting the cold box/photometer head unit with the electronics rack assembly. This system was inefficient in many ways and it was decided to redesign it and to construct a new system.

The system as used for these observations is shown schematically in fig. 3. The control logic and deflection generators are basically unchanged from the first system, except for the changes necessitated by the use of a different coil assembly. In addition, the video signal is now filtered above 10 kHz by a simple RC circuit at the input to the A/D converter in order to avoid aliasing problems with the

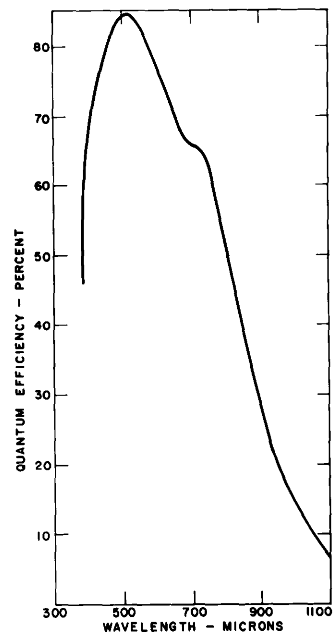

Figure 1
Target Quantum Efficiency

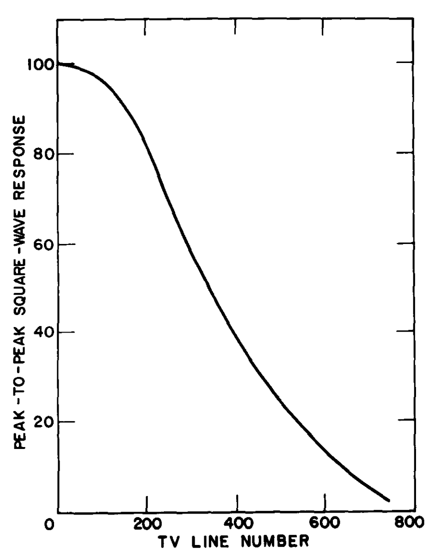

Figure 2
Target Modulation Transfer Function

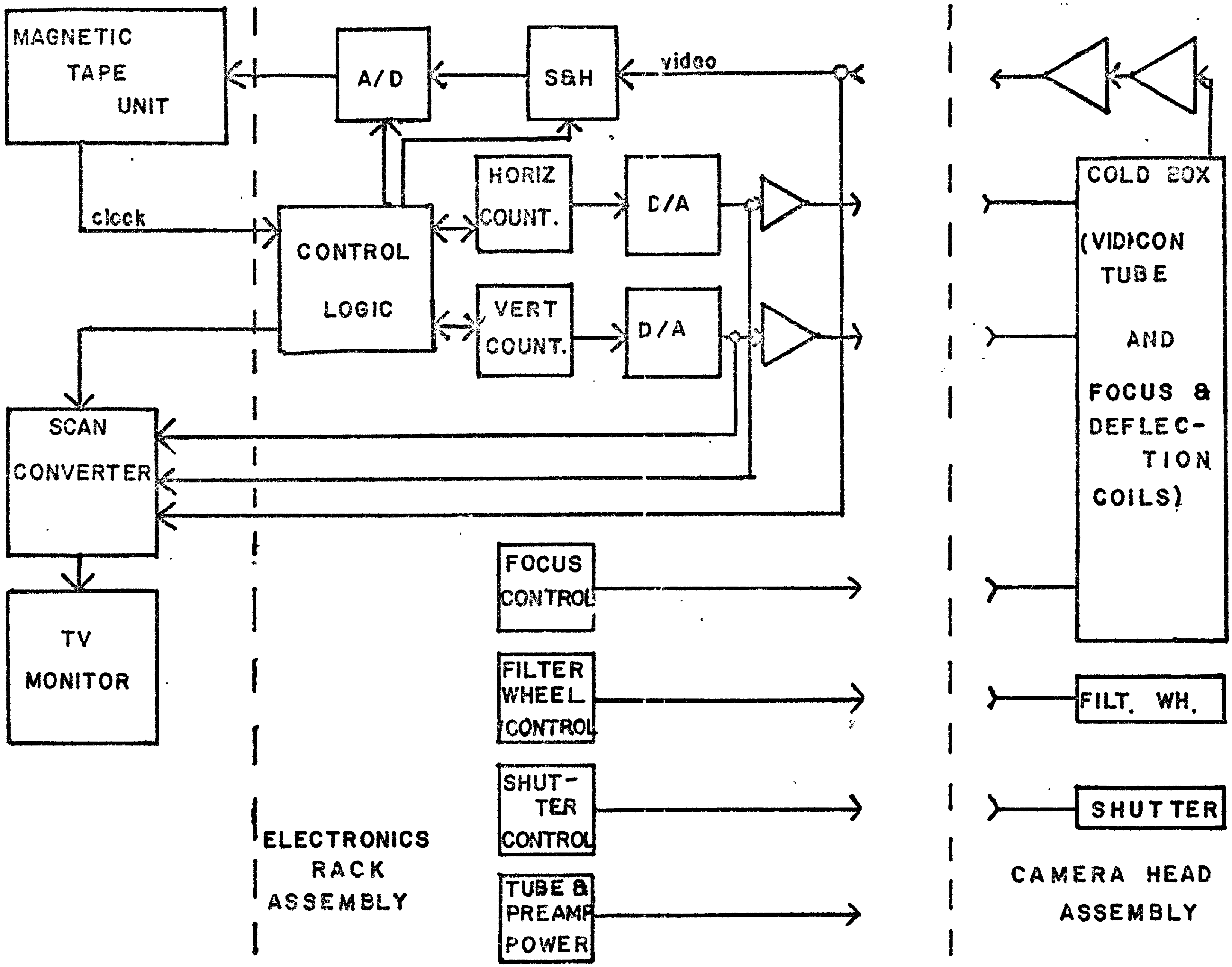

Figure 3. System diagram

20 kHz sampling frequency. The A/D converter is a 0-10 volt 10-bit unit, of which the middle eight bits are used. This allows each pixel to be recorded as one word on the 9-track magnetic tape with a resolution of 256 gray levels of about 19.5 mV each. In order to avoid ambiguity, the signal range is limited to less than five volts peak-peak. By recording an unexposed, or "dark", field immediately after the picture is read off the target, correction can be made for short-term drift in the preamplifier bias, thereby yielding a value between 0-5 volts which is digitized to a value in the range 0-255 for each pixel. Inasmuch as the system noise, in this case due to the preamplifier, is about 10 mV peak-peak, the noise in the digitized picture is limited by the $\pm$ 1/2 LSB digitization noise.

A major addition to the system was a Hughes scan converter unit, which consists of a storage tube and electronics which write an image onto the tube at the system's 3.3 second frame rate, and then read it off continuously at standard television rate into a 9" monitor. The scan converter provides an overall qualitative display of the data that have been recorded, which, in conjunction with a quantitative display on the oscilloscope monitoring the video signal, provides very effective feedback to the observer about the quality of the picture he is obtaining. This addition to the system can increase the observing efficiency many times by allowing the observer to retake bad pictures or avoid taking redundant pictures.

The main change in the system is in the camera head assembly, which includes all the equipment mounted on the telescope itself.

One major problem with the original system was the fact that the cold-box was merely a container in which dry ice was physically packed around the tube/coil assembly. In addition to the poor insulation of this device, the open assembly of the can allowed the faceplate of the tube to become fogged with water condensing onto the cold glass. In order to eliminate these problems, a standard photomultiplier-tube dry ice dewar was modified to hold the vidicon assembly. Thus the tube sits in a dry nitrogen atmosphere which is cooled by dry ice packed around the sealed N_2 container; the entire assembly is insulated by an outer vacuum chamber. The light beam enters the cold box through a sapphire window, which is heated to prevent condensation. The tube and coil assembly are connected to the main cable through an hermetically sealed connector. The video signal is fed from the tube target electrode through a coaxial cable to the preamplifier, which is mounted on the cradle holding the dewar; this cable is also sealed at the point where it enters the cold box in order to retain the integrity of the nitrogen chamber.

A 1 cm^2 black mask was placed on the faceplate of the tube to provide a reference for the initial setup of the system; it also acts as an aspect ratio scale in the data, as described in Chapter III.

The photometer functions of the camera were designed to make use by only one observer as easy as possible. A schematic is shown in fig. 4; the design in use is usable at any focal ratio up to f/3 without vignetting the 1 cm mask. Directly in front of the coldbox window is a wheel carrying 1-inch-diameter interference filters. The wheel is driven by a stepping motor (one step = 1.8°, 4-200 steps/

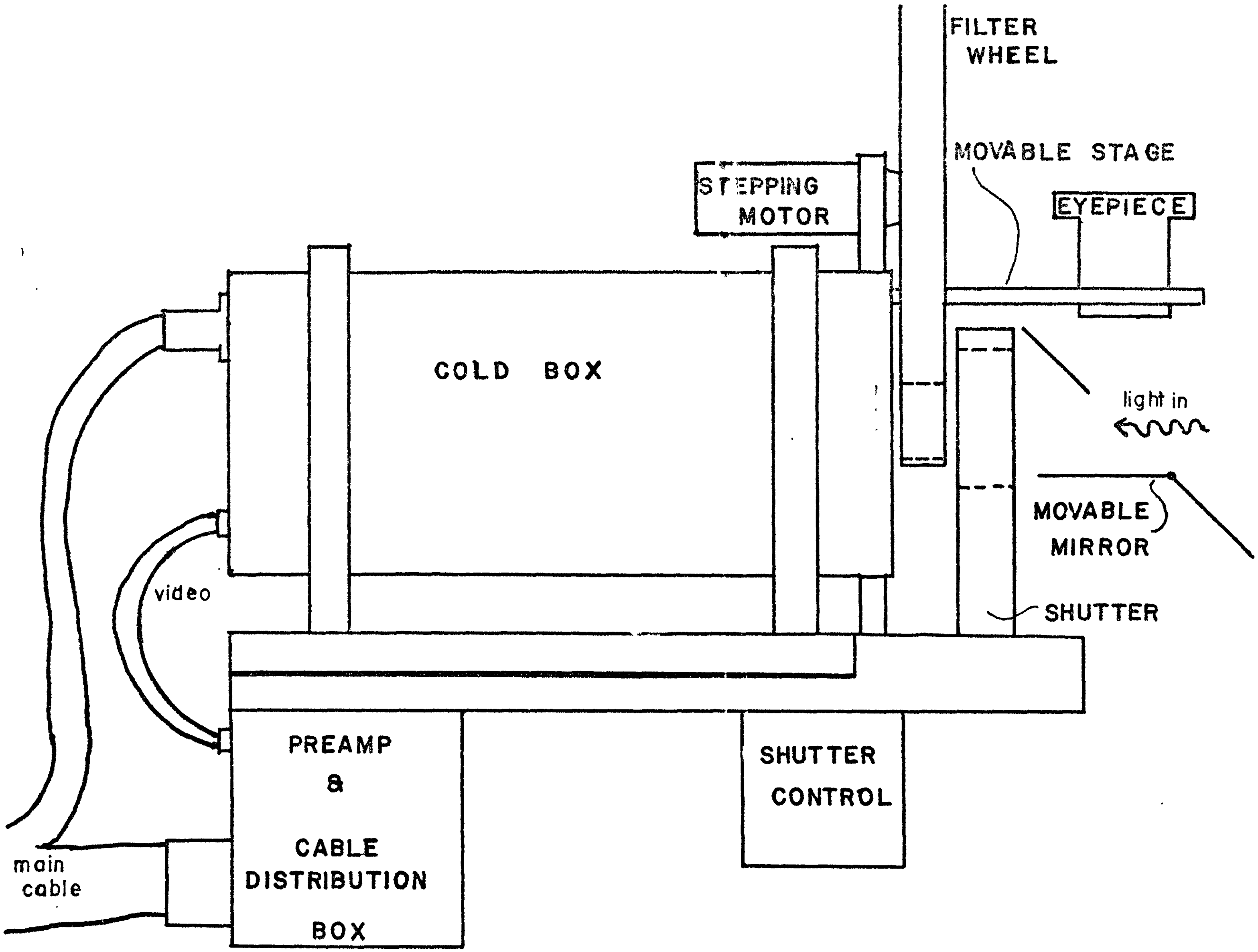

Figure 4

Camera head

second) which can be mounted to accommodate either a 25- or 33-hole filter wheel. A small hole is drilled at a known spot on the filter wheel and is used with a lightbulb/phototransistor system to detect a "home" position of the filter wheel. The observer can control the motion of the filter wheel from the panel; he can increment the wheel to the next filter in either direction, or move it to the home filter at any time. In this manner, it is possible to use any set or subset of filters in any order, with minimum waste of time.

In front of the filter wheel is a 2.5-inch-aperture Compur self-cocking electronic shutter. The control box for the shutter is attached to the dewar mount; it is controlled by a shutter timer in the electronics rack. The observer can time exposures from 0.01 seconds to 99.9 minutes by adjusting front-panel switches, or he can manually control the shutter's operation. This is a great improvement over the prototype system, which normally required a second observer to operate the camera shutter mechanism manually at the telescope. In addition, the shutter incorporates a continuously-adjustable iris diaphragm, which is useful as a light baffle when scattered light in the telescope tube is a problem.

Between the mounting ring and the shutter, a large (4" x 6") 45° mirror is fixed in place; an oval portion of the mirror, large enough to pass the image beam, is cut out and mounted to a motor, allowing the cutout to be moved into or out of the beam path. A movable eyepiece is mounted above the mirror, cofocal with the tube target, to allow viewing of the object for focusing when the center mirror is up, or offset guiding for long exposures.

In operation, the procedure is as follows: the desired filter is placed in the beam path, and the exposure is determined from trial and error or previous pictures; the correct exposure will give a video signal of five volts peak-peak on the oscilloscope. The scan converter is used to check placement, guiding, and focus. The tube is then erased and the shutter timer started. When the exposure is finished (monitored by a panel light), the tube target is read out simultaneously to the scan converter and to the A/D convertter and magnetic tape drive. The tube is erased, and a dark field is immediately recorded to correct for preamplifier bias as mentioned above. This is the sequence for each picture.

In order to correct for variable sensitivity across the tube target, it is necessary to record a uniform or "flat" field. It has been found that the best way to do this is to look at a portion of the daytime sky with the vidicon mounted normally on the telescope. In addition to providing a very uniform illumination across the field, this method has the advantage of using the same optical system as the data pictures, allowing such problems as dirt or scratches on the filter, et cetera, to be eliminated. In practice, flat fields are taken of the bright sky in the evening and/or morning of each observing night through each filter used.

Chapter III -- Data Reduction

Compared to standard photoelectric photometry, the vidicon photometer produces a very large amount of data. Each picture consists of 256 lines of 256 pixels each. Each pixel is represented by an eight-bit character on the magnetic tape. As was noted above, it is not difficult to take over one hundred pictures per night; one thousand per telescope run is not uncommon. Data reduction is done on the M.I.T. Laboratory for Nuclear Science IBM 360/65 computer, which, with less than 40,000 words of memory, puts many restrictions upon the software. A method had to be developed which provided a good compromise between efficiency and flexibility of operation.

The software system developed for this project combines the use of magnetic tapes as long-term storage, with disk packs for on-line use. Each disk holds approximately ninety frames of data, and all software which operates on the pictures uses data from the disk. The system incorporates functions which have been found to be necessary for standard processing, as well as special functions for odd-format or incorrectly-taken pictures. Also, any frame can be processed by a procedure written for a specific purpose, merely by including it as part of the input.

An example of raw data as it is read off the vidicon tube is shown in fig. 5. The mask on the vidicon can be seen fairly clearly, illuminated by the lunar scene being imaged. The structure along the edge of the picture is due to the "ringing" of the horizontal

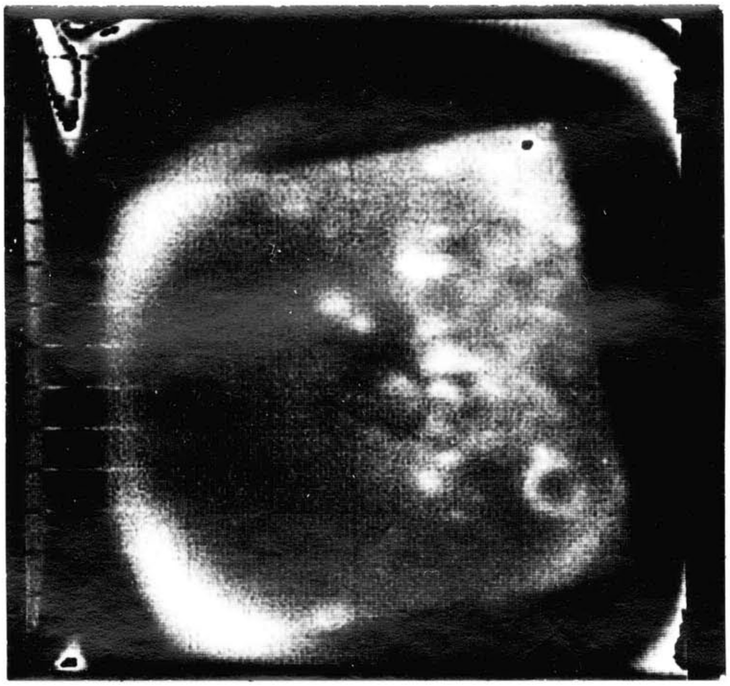

Figure 5
Raw data format

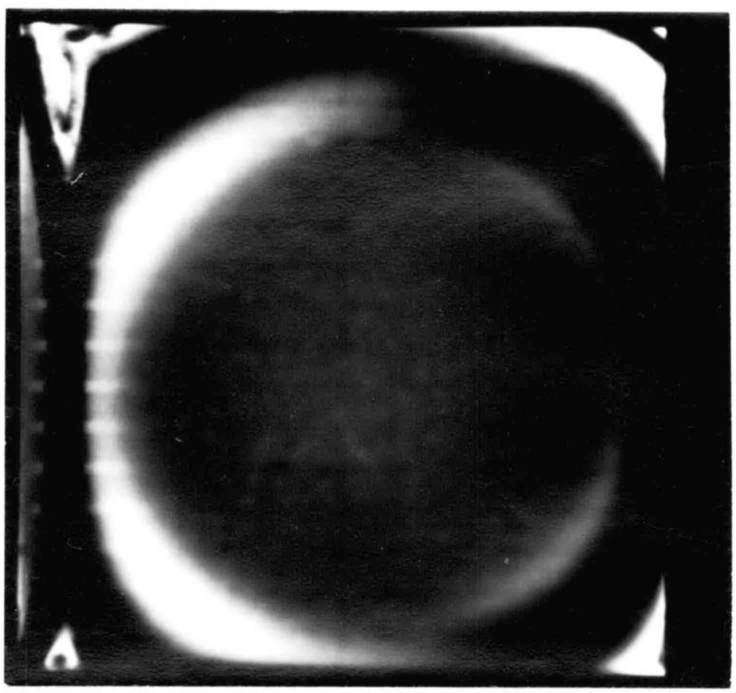

Figure 6
Dark Field

deflection coil immediately after flyback; the scan is adjusted to move the masked area out of the zone of the ringing effect. The horizontal lines are due to the stopping of the scan every sixteen lines while the tape recorder, which is clocking the scan electronics, is writing a record gap to separate data blocks. The circular structure evident in the picture is due to electrons scattered from the ring holding the target in place in the tube. It has been subsequently determined that this effect can be largely eliminated by lowering the electron beam current. The small dark spot within the mask is a bright crater which caused the video level to go above 5 V. However, as long as the peak-peak voltage in the picture does not exceed 5 V the information can be recovered.

Fig. 6 is a dark field taken immediately after the tube was erased of the preceding picture. This picture is at approximately the same bias level in the preamplifier, so that it can be subtracted from the data to yield a standard picture as described in Chapter II. This result is shown in fig. 7. At this time, the portion of the field outside the mask is set to 0.

As was discussed previously, each picture is corrected for differential sensitivity across the target through the use of a flat field. This frame also has the bias removed and the borders cleared. The flat field is then scaled in such a manner as to set the intensity at the center of the field equal to 1.00. Since the data of interest in the field are relative rather than absolute, this "normalization" makes the picture easier to handle without sacrificing data. An

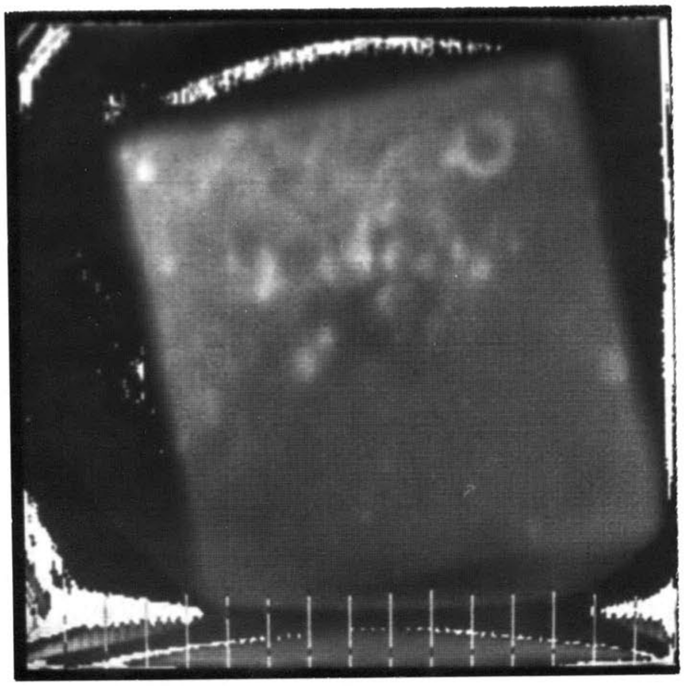

Figure 7
Dark field subtracted from raw data

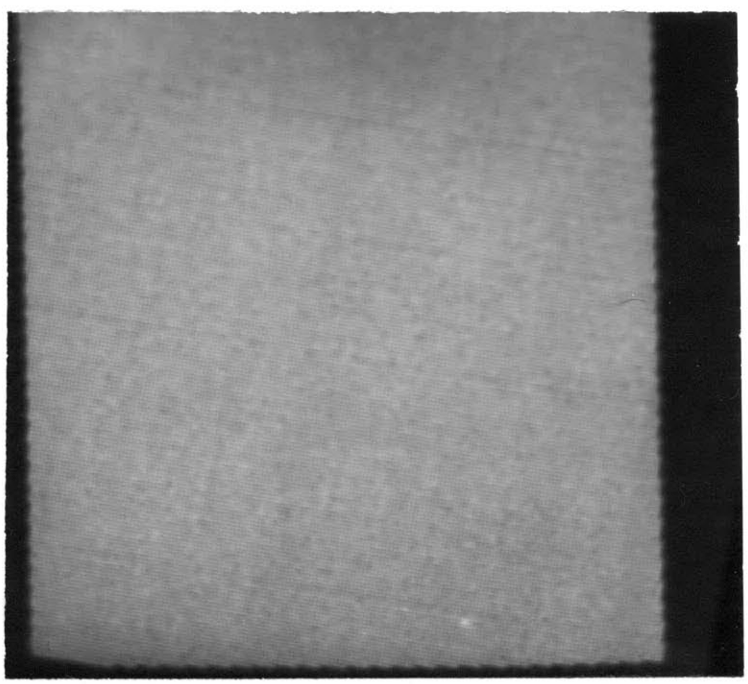

Figure 8
Normalized flat field

example of a normalized flat field is shown in fig. 8.

The final step in the basic processing procedure is the division of a data frame by the appropriate normalized flat field. This "corrected picture" is the basis for all further processing; each frame used is processed in the same way up to this point. The corrected example frame is shown in fig. 9. The printed numbers for a portion of this picture are followed through the processing in fig. 10.

Several additional steps suggest themselves as pieces of the basic processing system; they were not used for various reasons. Removal of low-level periodic noise through Fourier processing is a possibility; however, as has been noted, the digitization does not extend into the noise region where such a process would be useful. A system is currently being designed which will use a 12- or 14-bit A/D converter; with this system, extending the useful range of the data will be possible through the use of sophisticated noise-processing programs. Aspect ratio correction is another possibility. Using the mask, which is known to be square to an accuracy of better than 0.1%, it is possible to adjust scan controls in the hardware to give the correct ratio, or to measure this ratio from the appearance of the mask in the data and to correct by computer. The latter process was used to determine that the aspect ratio in the data under consideration is approximately 17:18, and it was decided that correction at this level was not significant. Finally, it should be possible to correct for geometric distortion caused by the scanning of the electron beam and other factors. This has been measured in the

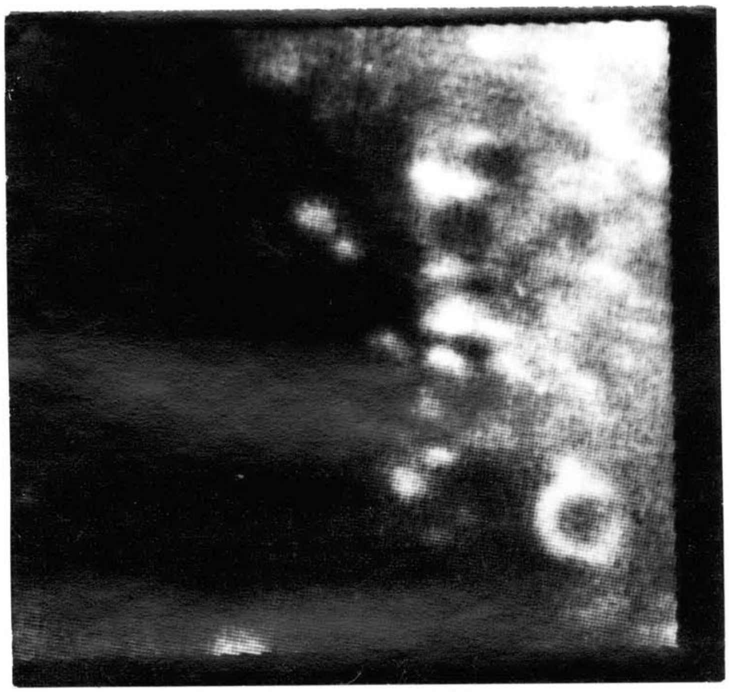

Figure 9
Example of corrected picture

IMAGE RAWDATA STRIP 1 X FROM 33 TO 55 Y FROM 120 TO 155

93	98	104	106	107	107	108	108	110	111	115	117	119	120	122	120	118	115	114	113	113	114	116
91	99	104	107	107	108	108	109	109	111	112	116	116	120	121	121	119	118	115	114	113	116	116
92	99	104	107	108	109	108	109	109	111	112	116	118	121	121	123	122	121	118	118	117	120	120
89	95	102	104	106	107	107	108	109	109	111	113	116	117	118	119	119	118	118	118	119	120	121
88	95	101	104	105	106	107	107	108	108	110	111	113	114	115	115	115	115	115	115	117	119	120
87	94	99	103	105	107	108	110	110	111	110	111	113	115	113	114	113	114	115	117	118	120	120
87	96	101	105	107	110	112	114	114	116	116	117	117	117	116	115	115	114	115	117	120	120	121
87	94	100	105	108	111	115	117	120	121	123	123	122	120	119	116	114	115	117	117	119	120	120
83	92	99	106	108	111	115	119	121	124	127	129	127	125	124	122	118	115	116	118	118	119	120
81	88	95	101	106	108	113	116	120	123	126	127	126	123	123	120	117	115	116	117	119	119	121
84	90	97	103	109	110	113	116	119	120	123	126	126	125	123	120	120	119	121	123	125	127	129
83	91	97	104	107	110	111	113	114	115	117	119	120	121	121	121	119	121	121	124	127	131	132
82	89	95	103	107	109	109	109	110	112	112	114	116	118	116	117	116	119	120	123	126	130	131
82	88	96	103	109	110	110	109	110	111	114	115	117	118	118	118	119	120	122	124	127	129	132
81	87	95	102	109	112	114	113	113	113	115	118	121	122	123	120	119	118	120	122	126	127	130
80	87	94	103	110	115	116	117	116	120	122	126	128	130	128	125	121	121	120	122	125	128	129
78	85	92	100	106	111	113	114	117	119	122	125	127	129	127	125	122	122	121	124	126	129	129
78	85	93	100	107	111	115	115	117	118	120	123	126	127	129	127	127	127	127	128	130	131	132
74	80	86	93	100	106	108	110	112	114	117	118	122	125	130	132	134	136	137	137	140	143	141
72	78	86	93	99	105	107	108	109	112	114	115	119	124	129	135	138	143	143	143	142	142	138
72	78	85	91	98	103	107	108	110	110	111	112	116	121	127	133	139	143	146	145	145	144	141
71	77	84	91	97	102	106	109	108	109	111	114	117	123	129	135	141	147	148	151	151	152	149
69	76	82	89	94	101	105	107	107	108	109	112	113	116	122	128	133	139	143	147	152	157	158
69	75	82	87	94	101	107	108	108	108	109	110	112	114	118	121	125	129	134	140	146	152	158
69	74	82	87	95	102	107	109	111	110	110	111	112	113	116	118	121	123	127	131	137	142	147
61	67	74	80	88	95	101	103	103	103	105	105	106	106	108	109	113	115	119	122	127	130	134
67	73	79	84	93	99	106	108	110	109	111	110	112	113	115	115	120	123	127	129	132	134	136
66	73	80	87	94	102	107	110	112	111	111	111	111	112	115	118	122	126	130	132	135	136	137
66	73	79	85	92	101	107	112	112	113	112	113	114	116	118	121	126	130	133	135	135	136	133
66	72	79	85	93	100	107	112	115	114	114	114	116	117	118	120	125	129	134	135	135	133	133
65	72	78	85	92	99	106	113	115	116	116	117	117	119	121	124	128	133	137	138	138	136	135
67	73	80	86	93	100	108	114	117	117	117	117	120	121	125	128	132	135	139	139	140	141	140
66	72	78	85	91	99	107	113	117	118	118	119	120	124	126	130	133	136	139	141	141	143	141
65	71	77	83	90	98	106	113	118	119	119	121	122	125	127	130	132	134	136	139	141	141	140
65	71	77	85	90	99	106	114	120	124	125	126	126	129	130	134	135	137	138	140	141	142	139
67	72	79	85	93	100	110	117	125	128	130	131	133	134	136	136	136	136	138	140	142	140	137

Figure 10a. Section of raw data frame

IMAGE DARKSUB STRIP 1 X FROM 33 TO 55 Y FROM 120 TO 155

53	58	63	66	66	66	66	68	69	69	72	74	74	76	77	75	73	71	68	67	66	68	69
51	60	64	68	67	68	66	68	67	69	69	74	73	77	77	77	74	74	69	68	65	69	68
51	58	63	66	66	67	66	67	67	68	70	72	75	78	77	79	78	76	73	72	71	73	73
50	55	61	62	65	66	66	65	67	67	69	70	73	73	75	75	75	73	75	73	74	73	74
46	54	59	62	63	65	65	65	65	66	66	68	69	71	71	71	70	70	69	69	71	73	73
46	54	58	63	63	66	66	69	68	69	68	69	69	71	68	69	67	70	70	72	71	73	72
47	56	60	65	66	69	70	72	72	73	72	74	73	73	72	71	70	69	70	72	74	74	75
47	53	59	64	67	69	74	75	78	78	81	80	79	75	74	70	69	70	72	70	72	72	73
41	51	58	65	66	69	72	77	77	81	84	86	83	81	80	78	74	71	72	73	72	73	72
45	51	59	65	71	71	77	79	84	86	89	90	89	85	85	81	78	74	75	75	77	75	77
44	50	57	63	69	69	72	74	77	79	81	84	83	83	81	78	76	76	76	78	79	81	81
42	50	56	64	66	69	69	71	72	73	75	76	78	78	78	77	75	75	75	78	81	84	85
41	49	54	62	65	68	66	68	68	71	70	72	73	76	73	74	72	76	74	78	79	84	83
42	48	55	62	68	69	69	68	68	69	72	72	74	75	75	75	75	76	77	79	82	83	85
40	46	54	60	68	71	73	71	71	70	73	76	79	80	80	77	75	74	76	77	80	81	83
38	45	52	61	69	73	74	73	72	74	77	82	85	86	85	80	77	76	75	75	78	80	81
36	43	49	58	63	68	70	72	74	77	78	81	83	86	82	80	76	77	75	77	78	82	81
36	44	52	59	65	69	73	73	74	75	76	80	82	84	84	83	82	81	80	81	82	84	84
33	38	44	51	58	63	67	68	71	71	75	75	80	82	87	88	90	91	91	91	93	95	94
31	36	44	50	56	62	64	64	65	67	70	70	75	78	84	89	91	95	96	95	94	93	90
30	36	42	48	55	60	64	65	66	67	68	68	72	77	82	89	93	97	99	98	96	97	92
28	34	40	47	54	59	62	66	64	65	67	70	72	79	84	90	94	101	102	106	104	105	100
27	32	39	46	51	58	62	63	65	65	66	68	70	71	78	83	89	93	97	100	105	109	111
27	32	39	44	51	57	64	64	64	64	65	66	68	69	73	75	79	82	86	93	99	104	109
26	31	39	43	51	56	62	63	65	64	65	66	67	67	71	73	75	77	80	84	90	94	99
25	30	38	43	51	57	63	64	65	65	67	66	68	67	69	68	72	73	79	80	85	87	91
23	29	35	41	49	55	61	65	66	66	68	67	68	69	71	71	74	76	79	82	84	87	88
23	30	37	44	50	56	62	65	68	67	67	67	66	67	71	73	77	80	85	86	88	89	89
20	27	34	40	47	55	61	67	66	69	68	69	69	71	72	75	80	84	87	90	88	90	85
22	28	34	39	48	55	63	67	72	70	71	69	71	70	71	73	79	82	87	88	87	85	84
19	26	32	39	45	53	60	68	68	70	69	71	70	71	73	76	79	84	87	89	89	87	86
20	27	34	40	47	54	62	68	71	71	71	71	74	76	79	83	86	89	92	92	92	93	91
20	26	32	38	45	52	60	66	71	72	72	73	74	78	80	84	87	89	92	94	93	96	94
19	23	29	35	44	51	60	66	72	72	73	74	76	78	81	83	85	86	89	91	94	93	92
18	25	30	38	42	50	57	66	72	76	77	79	79	81	82	86	86	87	89	91	91	93	90
19	25	30	36	43	52	60	68	77	80	81	84	86	87	89	89	88	89	90	92	93	91	88

Figure 10b. Section of raw data with dark field subtracted

IMAGE CASS.402 STRIP 1 X FROM 33 TO 55 Y FROM 120 TO 155

69	74	80	84	84	85	84	87	88	89	91	93	92	96	94	92	88	87	82	80	78	79	80
67	78	84	88	88	87	85	87	86	88	89	93	92	97	96	94	91	90	84	82	78	82	80
67	75	81	86	86	87	85	87	87	87	88	91	94	97	94	97	95	92	88	86	84	87	86
65	71	79	80	84	86	86	84	86	85	88	88	92	90	93	91	91	88	91	87	88	86	87
59	69	76	79	80	83	83	84	82	83	82	84	84	85	84	84	82	83	81	81	82	84	84
0	69	73	80	80	83	83	86	84	85	84	84	83	85	81	82	80	82	82	85	83	84	83
0	73	77	84	85	90	88	92	91	92	90	92	89	90	88	86	83	82	82	85	87	86	87
0	67	75	81	84	85	92	93	96	95	99	96	94	88	87	82	81	80	83	81	83	83	84
0	65	74	84	86	89	94	98	98	102	106	107	103	99	98	95	89	84	86	88	86	85	84
0	66	75	84	90	90	97	100	105	108	110	111	109	103	103	99	95	89	88	89	90	88	89
0	63	71	79	85	85	89	92	94	98	97	102	100	100	95	92	89	90	88	90	91	94	92
0	64	70	79	82	85	85	87	88	88	91	91	94	92	93	90	88	88	88	91	95	96	98
0	0	67	77	80	83	82	83	83	66	85	86	87	90	86	86	84	88	86	89	91	95	95
0	0	68	76	83	84	84	82	82	83	86	85	87	88	88	88	88	89	89	91	93	94	97
0	0	67	74	83	88	89	87	85	84	87	91	94	94	93	90	87	86	88	89	92	93	94
0	0	63	74	84	88	90	88	87	88	92	97	101	101	100	93	89	87	88	87	90	91	92
0	0	60	71	77	83	86	87	90	92	94	96	98	100	96	93	88	88	87	89	90	95	95
0	0	65	72	79	84	89	88	91	90	92	95	98	99	99	97	95	93	93	93	95	96	97
0	0	0	63	71	77	80	82	85	85	88	89	93	97	102	101	102	104	104	104	106	109	107
0	0	0	62	68	76	78	78	79	81	85	84	90	93	99	104	106	110	111	110	109	107	103
0	0	0	59	67	72	77	79	80	80	81	81	85	91	96	103	109	113	115	113	110	111	105
0	0	0	58	67	71	76	80	78	77	80	82	86	92	98	106	112	117	120	124	122	121	115
0	0	0	57	62	70	75	76	79	78	79	81	82	84	91	97	103	107	111	115	121	125	126
0	0	0	54	62	70	77	77	76	76	77	78	79	81	85	87	91	95	100	108	115	118	124
0	0	0	0	59	66	72	74	75	74	74	76	76	76	81	83	85	87	90	95	101	106	111
0	0	0	0	63	70	78	78	79	79	80	79	81	79	82	80	84	85	92	93	99	101	105
0	0	0	0	58	65	72	77	77	77	79	77	77	79	81	81	85	87	91	94	96	100	100
0	0	0	0	60	66	74	77	80	78	78	77	76	77	81	84	88	92	98	99	102	102	101
0	0	0	0	56	65	73	79	78	81	79	80	80	81	83	85	91	95	101	103	102	103	98
0	0	0	0	57	65	73	78	84	82	82	80	81	80	81	84	90	93	100	102	100	97	95
0	0	0	0	0	62	69	79	79	82	79	81	79	81	83	86	90	95	99	102	101	99	98
0	0	0	0	0	62	72	79	81	81	81	81	84	86	89	93	97	101	105	105	105	105	103
0	0	0	0	0	60	69	76	82	83	83	83	84	89	91	95	99	101	106	107	107	109	107
0	0	0	0	0	58	68	75	82	83	83	84	86	89	92	94	97	97	100	103	106	106	103
0	0	0	0	0	57	65	75	82	86	87	90	90	92	93	98	97	98	100	103	103	105	101
0	0	0	0	0	59	68	77	87	91	92	95	98	99	101	101	100	101	101	105	105	103	99

Figure 10c. Section of corrected picture

laboratory where it was determined that such distortion was small to undetectable at the current resolution. Therefore this correction, too, was unnecessary.

In order to obtain the results needed for the project, it was necessary to devise an algorithm to divide two pictures. This procedure, which is simple in theory, was complicated by the severe storage limitation in the software system which necessitated the use of only 8-bit integers for storage. Nevertheless, a routine was developed which can divide any portion of any two pictures, and enhance the ratio obtained for easier visual display of the data, if desired. In addition, the actual ratios can be written onto a tape for use in programs which are not restricted to the integer format. An example is shown in figs. 11, 12 and 13. Fig. 11 shows the corrected figure previously seen and a similar one, taken at a different wave-length. It is clear that it is necessary to translate one picture so as to move the features into registration with the same features on the second picture. This is done by determining the brightest point on both pictures and assuming that they are the images of the same point. This was done by looking at the numerical printouts in the current case, although it could be done just as easily by the computer. This method is most easily used on a picture of the type illustrated, which shows sharp contrasting details. If the details are blurred or of low contrast, the method becomes more difficult, as with some of the data presented in Chapter IV. In the extreme case, it becomes

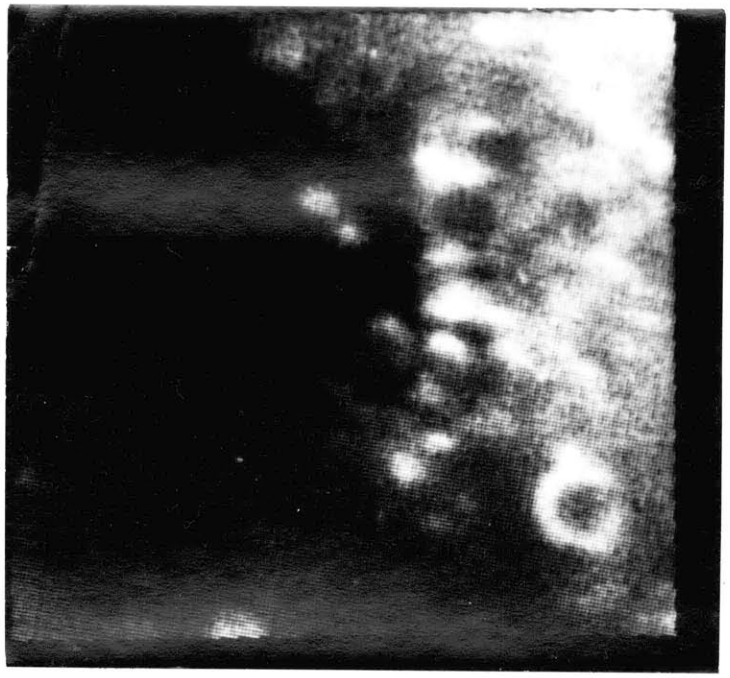

Figure 11a
Numerator picture

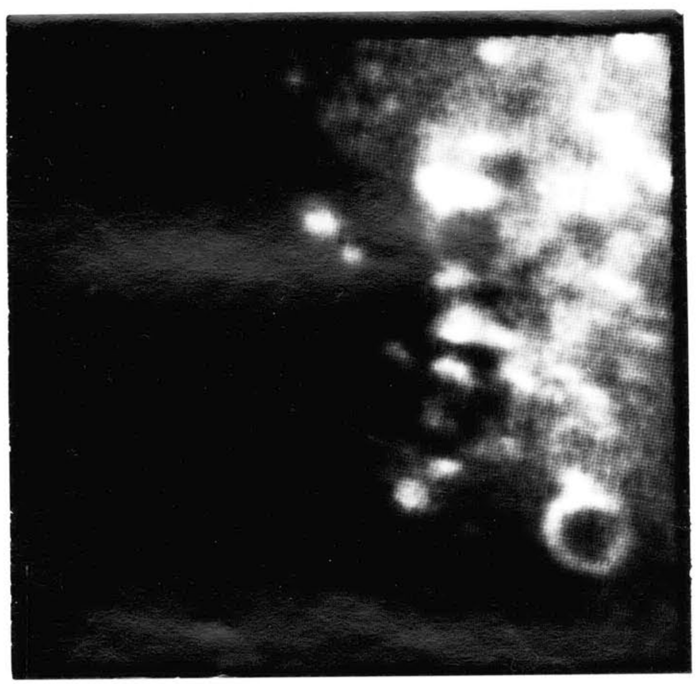

Figure 11b
Denominator picture

Figure 11c

Numerator frame. Contours at every 10 data number level. Higher numbers indicate brighter areas.

Figure 11d

Denominator frame

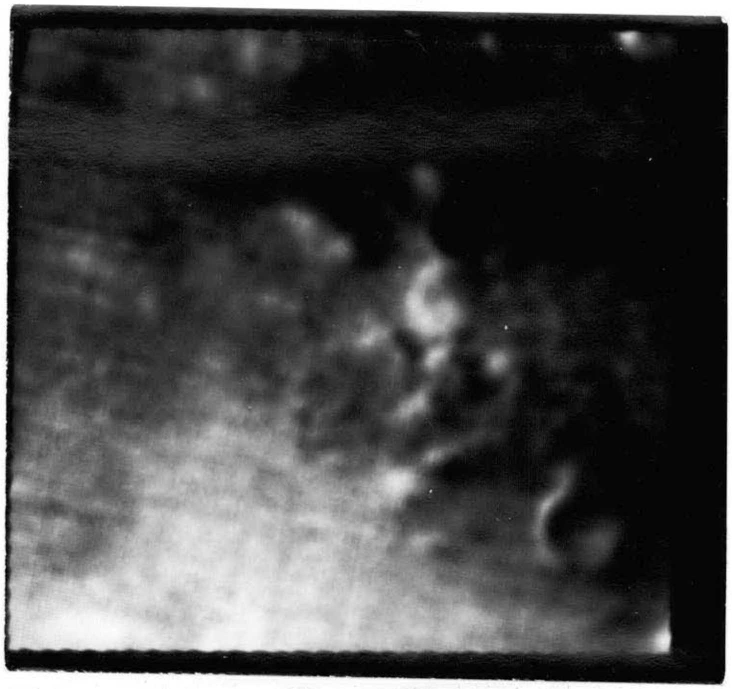

Figure 12
Ratio picture

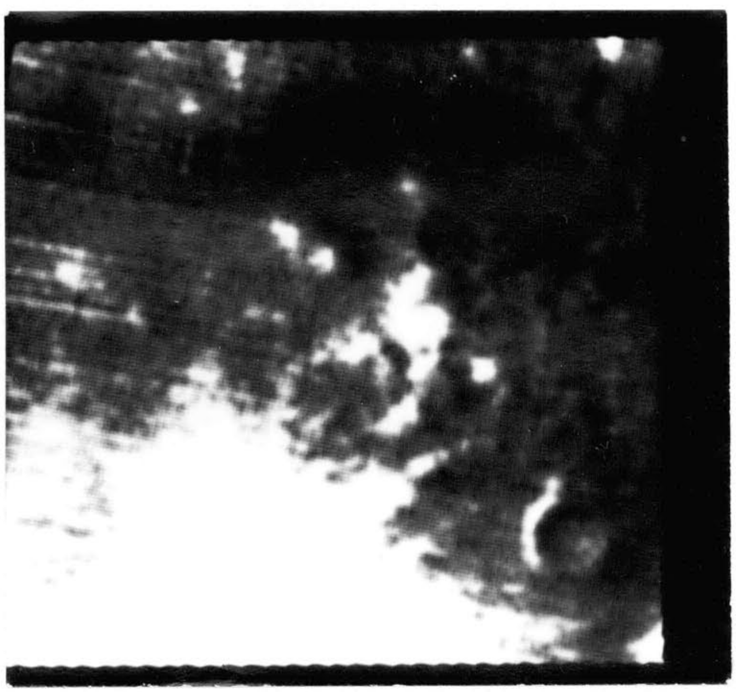

Figure 13
Ratio picture enhanced

necessary to determine the overlay either completely by eye or through the use of very sophisticated computer programs.

Although it is easy and generally sufficient to translate a picture in order to overlay it on another one, a rotation is sometimes also necessary. This type of correction, which is conceptually trivial, gives rise to distortion when performed on the discrete matrix produced by the vidicon, if interpolation is to be avoided. In this project, rotation was a concern only in pictures taken at the Coudé focus of the telescope; for reasons discussed in Chapter IV, such rotations of the data were ignored.

Fig. 12 shows the ratio of the two pictures in fig. 11. Each pixel in the ratio picture represents the element at the same coordinates in the numerator, divided by the appropriate element in the denominator, which has been translated to match features. This result is then multiplied by a scaling factor. In processing fig. 12 and other ratios in this work, the scaling factor was determined by giving the computer an arbitrary point in the ratio picture and defining that point as 1.0. In the picture, a light area represents an area where the numerator is brighter than the denominator, relative to the point where the brightnesses are defined as being equal; a dark area, accordingly, represents the denominator brighter than the numerator. It is seen that shifting the scaling factor, either by setting the normalization point value equal to something other than 1.0, or by choosing a different point, will change only the gray level representation of the ratio; the features will be the same. In other words, the isophots will remain constant and only their numerical values will change.

An enhanced version of the ratio is shown in fig. 13. The enhancement process multiplies numbers greater than 1.0 by a constant factor and divides numbers less than 1.0 by the same factor. The ratios are then converted to the 0-255 representation used in producing the pictorial display in such a manner that ratios which were near 1.0 are fully enhanced, at the expense of those ratios which were either very large or very small. The enhancement factor in fig. 13 is 1.25. The contrast is obviously enhanced in the areas which were close to 1.0, or halfway between black and white in the original ratio, while very bright or very dark areas are basically unchanged. Note that the horizontal structure caused by the record gaps is still somewhat visible. If this effect is not completely removed by subtracting the bias frame, then dividing two frames tends to enhance it. As the image moves within the frame from one picture to the next, it must be registered, while the horizontal lines, which are constant with respect to the sampling raster, are offset and show up in the ratio.

Chapter IV -- Observations

As mentioned in Chapter I, many studies have shown that differences in spectral reflectivity of areas of the lunar surface in the visible and near infrared regions can indicate significant mineralogical differences. Relative reflectivities in particular are very sensitive indicators of such differences; in addition, ages of surface features can be inferred from the shapes of the relative curves (McCord, et al., 1972). It is clear that accurate two-dimensional reflectivity studies can be of great importance both in obtaining data in unmeasured areas and in suggesting areas where further intensive observations would be of the greatest value.

The filter photometry in the previous works has produced accurate curves in the 0.3-1.1μ range through the use of over twenty filters. Such a procedure takes a significant amount of observing time for each area measured. While the vidicon photometer can make a measurement through the same filter in less time due to its higher sensitivity, it is in fact simultaneously measuring tens of thousands of discrete spots. To repeat this procedure for two dozen filters is possible, but the amount of data that would have to be handled would be overwhelming; displaying it all simultaneously would require a four-dimensional plot or picture. Therefore, the two-dimensional data is most efficiently used to map gross differences in the reflectivity curves, leaving intensive investigation to standard photometry. Dividing two pictures taken through any two different filters is a simple task; by carefully choosing from the set which pair of wavelengths to ratio, a number of different effects can be investigated. One of the advantages of the vidicon photometer for this kind of work is its standard, easily-handled output format. Another is the fact that dividing two pictures taken with the same instrument eliminates many effects that must be considered when dealing with two photographs, especially if different photographic emulsions are used, as in the blue and infrared. Additionally, the vidicon is more sensitive and potentially more accurate than photographic processes.

The site chosen for observations intended to test the system was the Mare Serenitatis/Littrow area, which includes the Apollo 17 landing site (see figs. 14-15). Data were taken on the nights of April 24-28, 1972, on the 84-inch telescope at Kitt Peak. The Coudé focus was used on the first night; on subsequent nights the instrument was mounted at the Cassegrain focus. The Coudé plate scale is 3 arcsec/mm and the Cassegrain scale is 12 arcsec/mm; with the vidicon scan set to about 180 samples across the 1-cm mask, the resolution limit is approximately 1/6 arcsec and 2/3 arcsec, or 1/4 km and 1 km respectively on the Littrow area of the moon. This resolution is, of course, theoretical; the seeing blur is the normal limitation. On the nights these data were obtained, the seeing was approximately 2 arcsec, so that the blurring is noticeable on the low resolution pictures and severe on the high resolution pictures.

Pictures were taken using four filters -- two in the visible, centered at 0.402μ and 0.564μ ($\Delta\mu$= 0.03μ), and two in the near infrared,

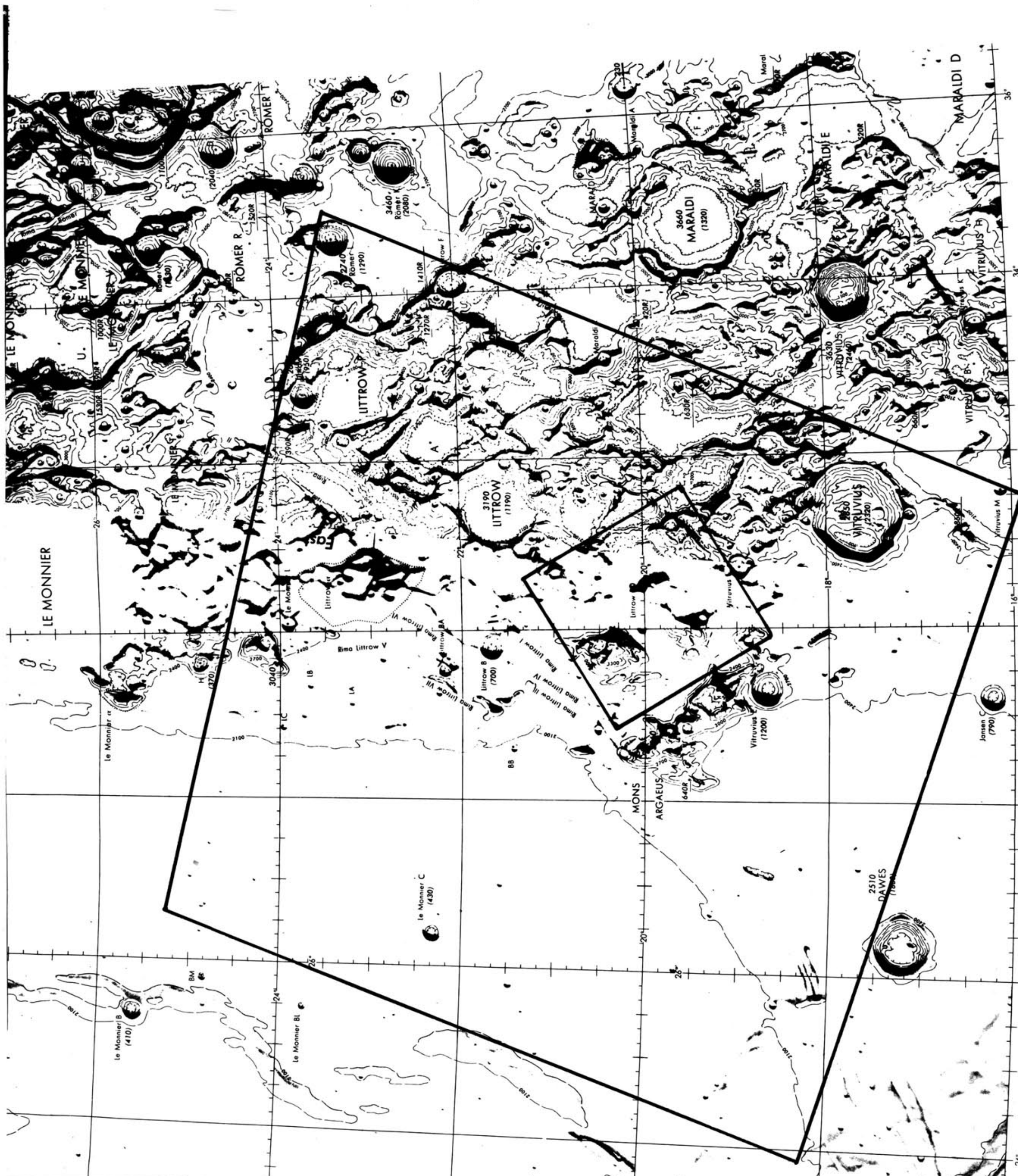

Figure 14
Portions of Lunar Aeronautical
Charts 42 and 43, showing
areas imaged in data pictures

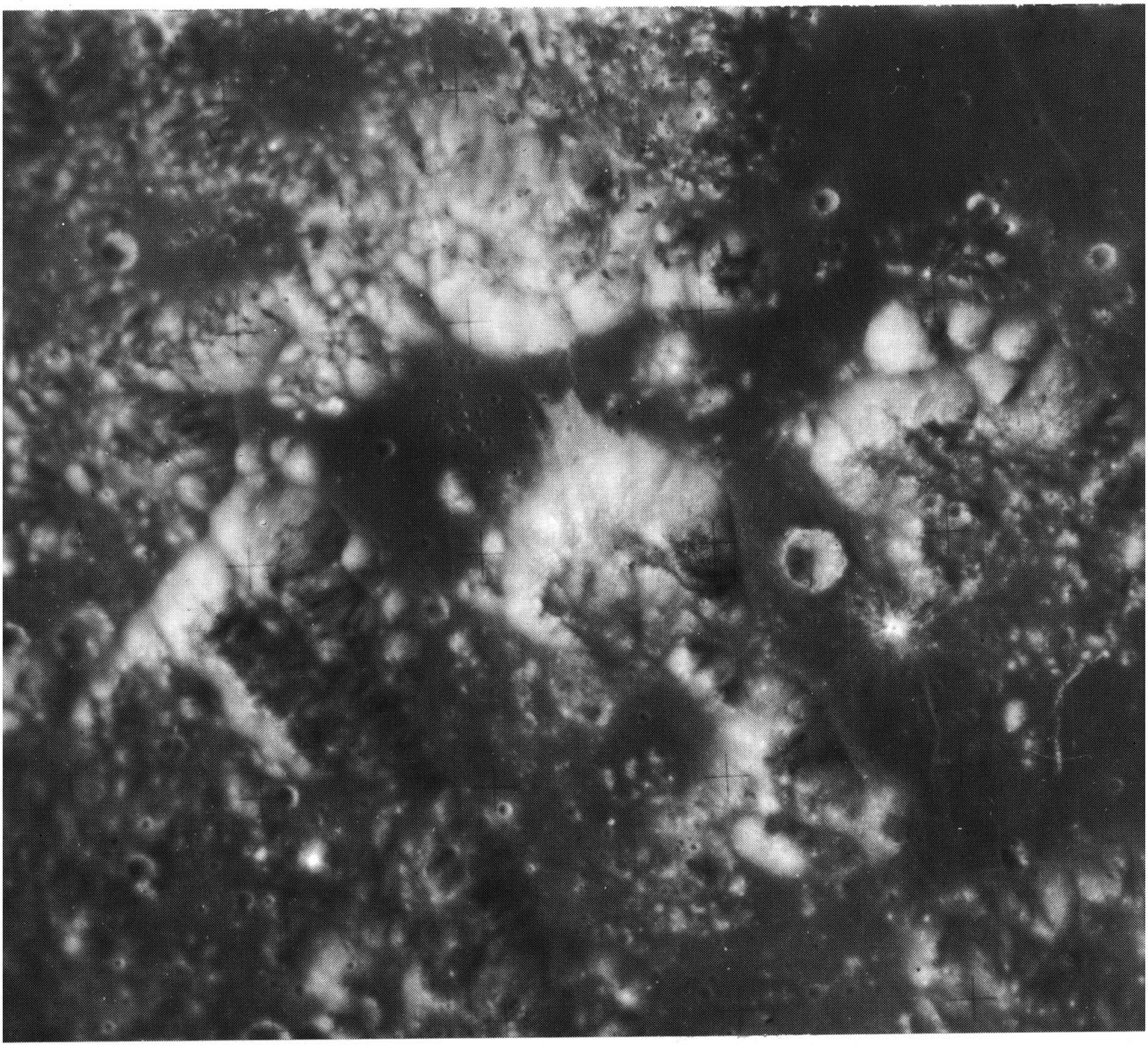

Figure 15
Picture of Apollo 17
landing site and surrounding
area, taken from Apollo 15

at 0.906μ and 0.948μ ($\Delta\mu$ = 0.05μ). One set each of four Coudé and four Cassegrain pictures was chosen for use in this project. In addition, two extra Cassegrain pictures were used as a check of the system, to determine the repeatability of results. Ratios were made of the following pairs of wave lengths: 0.402μ/0.906μ; 0.948μ/0.564μ; and 0.948μ/0.906μ.

The low resolution pictures are shown in figs. 16-19. The pictures encompass an area from the crater Vitruvius northeastward to the bright crater Römer L and west into Mare Serenitatis. It can be seen that although exposures are slightly different, albedo features repeat in all pictures.

Fig. 20 is the 0.402/0.906 ratio. The point which has been set to 1.0 is marked on the picture; the same point is used as the normalization, or standard, point in all the Cassegrain ratios, and the color differences shown are therefore relative to that point. Fig. 20 shows the southwestern area to be bluer by about 30%, with a steep gradient northeastward. The blue bright crater appears in the upper right, surrounded by material which is redder than the standard area by about 30%.

The 0.906/0.948 ratio is displayed in fig. 21. As expected, the raio is fairly constant across the field, to within ± 10%. The 0.948/0.564 ratio in fig. 22 again shows the crater in the northeast corner to be bluer by about 30% than the surrounding area, by as much as 40%, indicating a higher albedo in the green than in the infrared.

There is, however, an area in the center where the red is brighter by up to 20%. This is seen more clearly in the enhanced picture. In all ratios, the linear horizontal structure is introduced by the vidicon scanning system, rather than by any lunar features.

The high resolution Coudé pictures are shown in figs. 23-26. Because of the much smaller areas imaged in the pictures, the effects of seeing are much more evident; a 1 1/2 arcsec seeing blur encompasses an area of over 80 pixels. Therefore, small features on the ratios are not necessarily of great significance. Because of the drift of the image in the field between the taking of the two pictures, the ratios cover a correspondingly smaller area -- only those points which appear in both pictures can be divided. There is, in addition, a motion due to rotation of the image in the Coudé focus. However, because of the large spreading of areas in the picture, and because no two pictures which were divided were taken more than fifteen minutes apart, rotation of the images before overlaying was not done.

Figs. 27-29 are the three ratios of the Coudé pictures, with an enhancement of each. Again, there is a general cancellation of albedo features. Also, several features repeat, as expected, in the blue/red and red/green pictures. The 0.402/0.906 ratio shows a range of values from about 30% bluer to 20-25% redder than the standard area. The 0.948/0.564 ratio also shows less reflection in the infrared than in the visible, except for a few areas which are 10-15% brighter in the infrared than in the green, relative to the

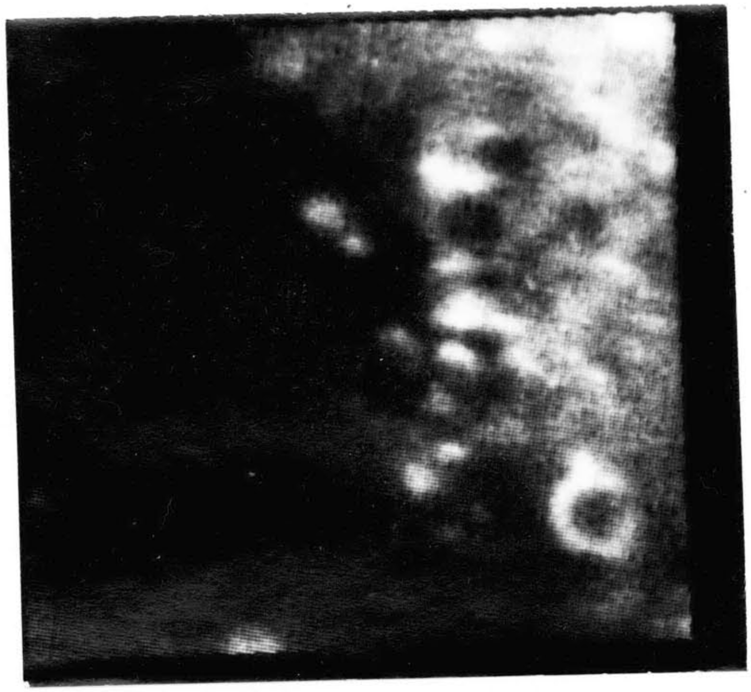

Figure 16
0.402μ, 0.22 sec exposure

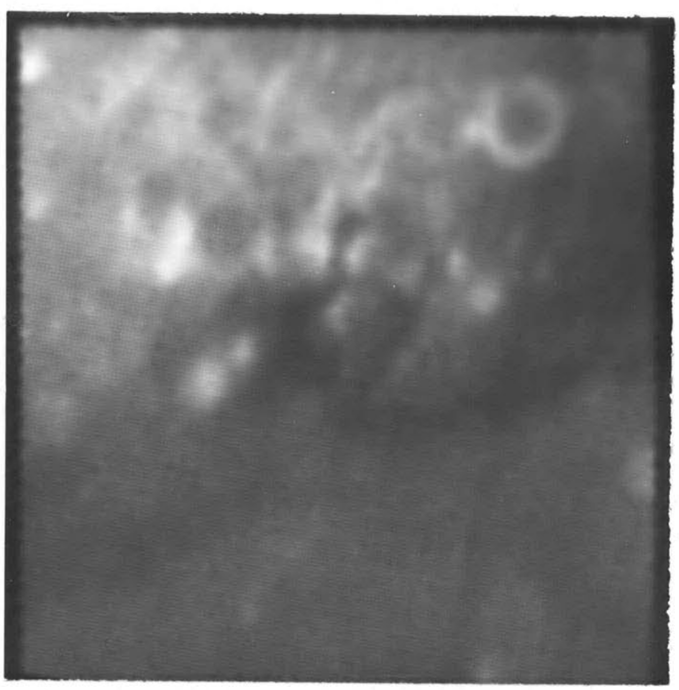

Figure 16
0.564μ, 0.08 sec exposure

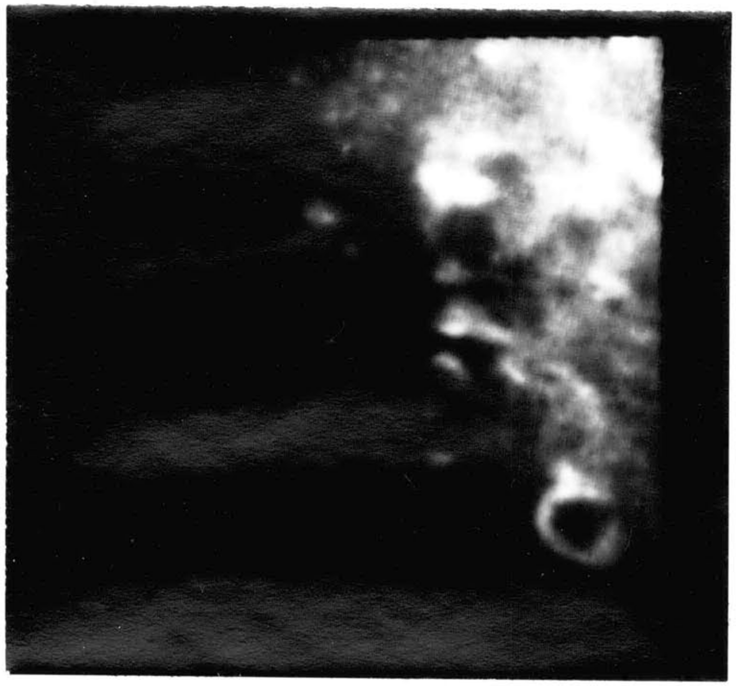

Figure 18
0.906μ, 0.12 sec exposure

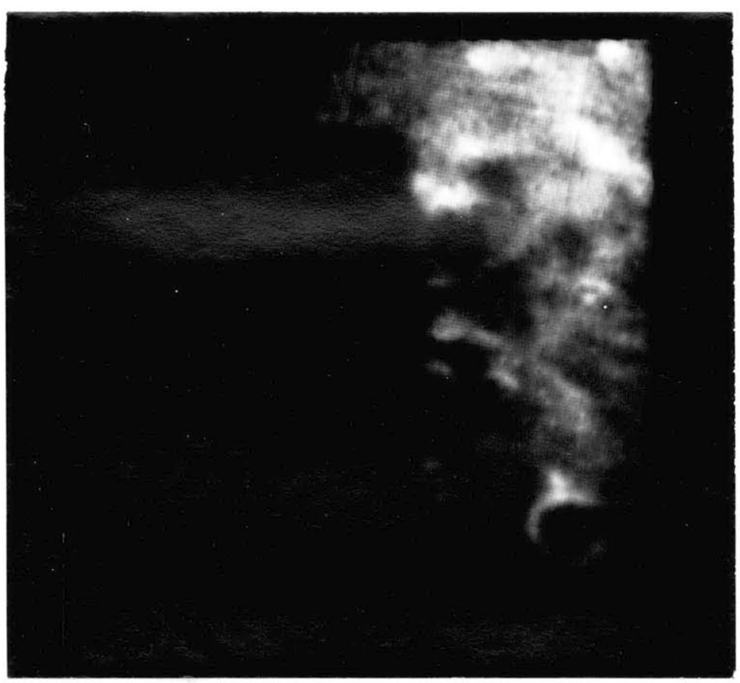

Figure 19
0.948μ, 0.14 sec exposure

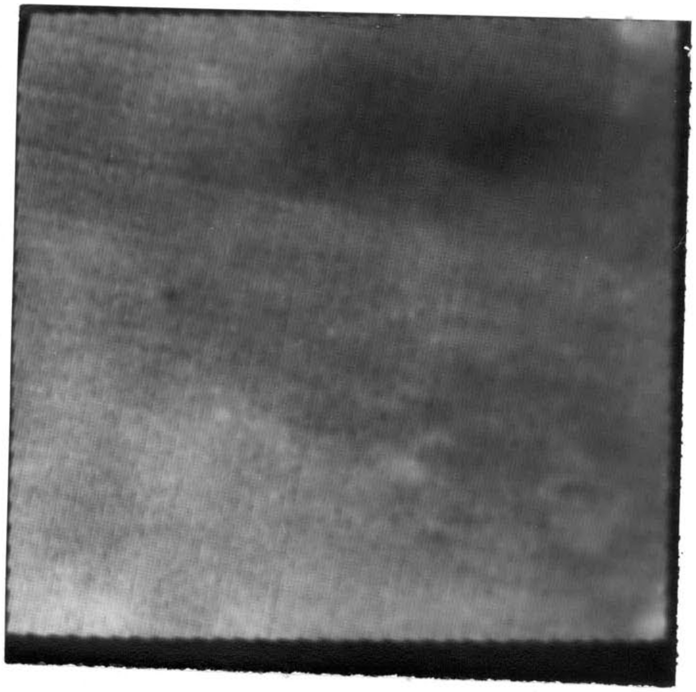

Figure 20a
0.402/0.906 ratio

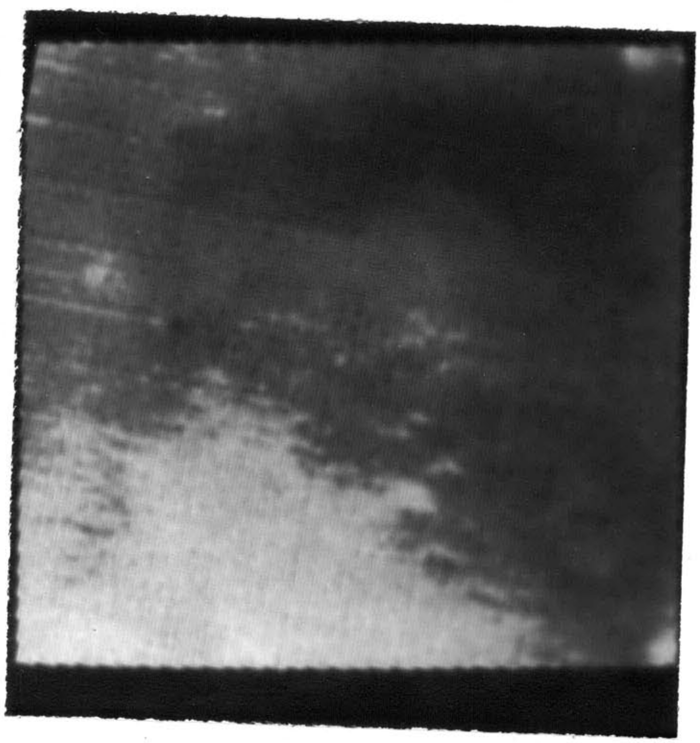

Figure 20b
0.402/0.906 ratio enhanced

Figure 20c

In this and subsequent ratio contour plots, contour levels are at 10% intensity variation levels

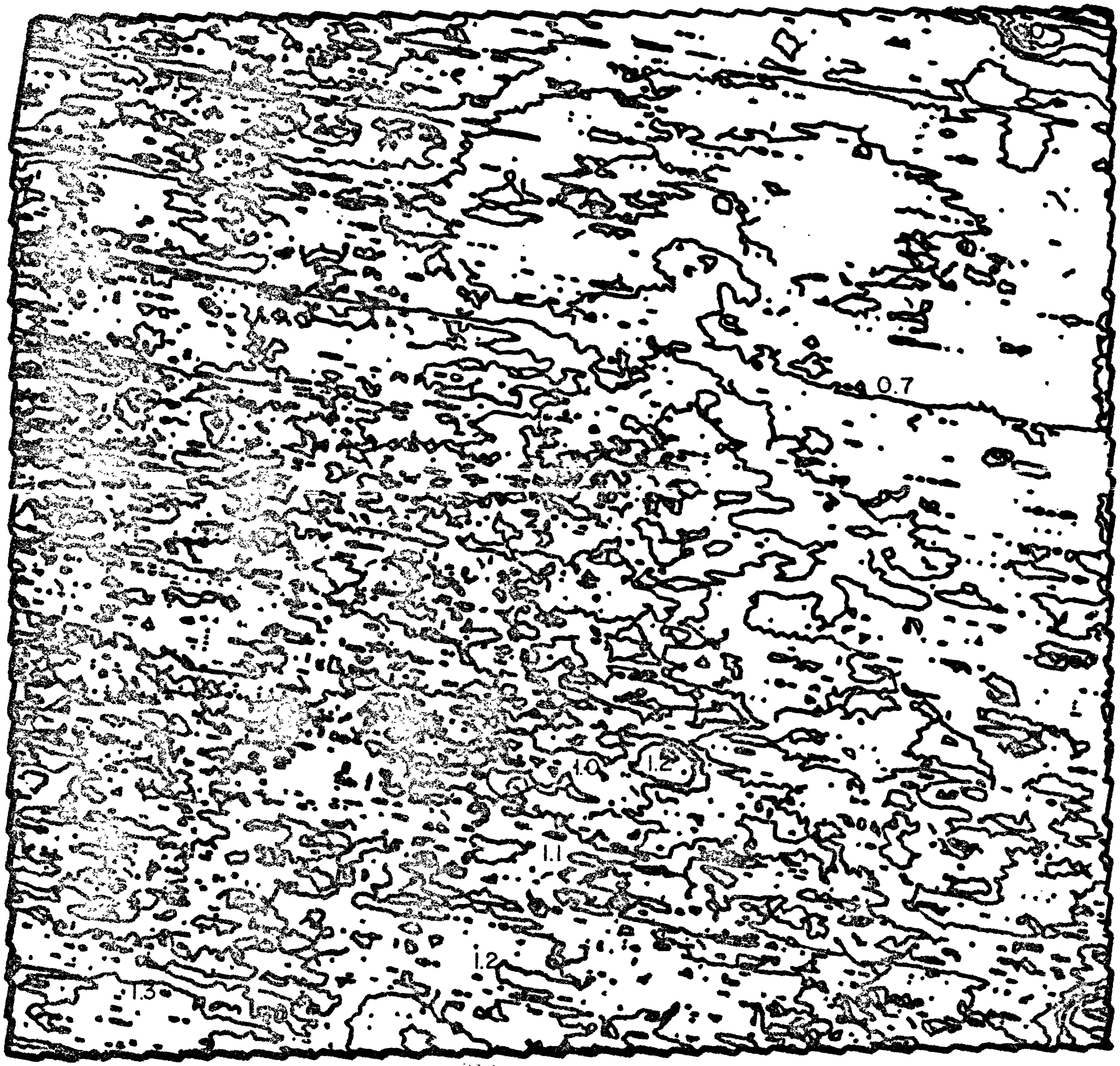

20c

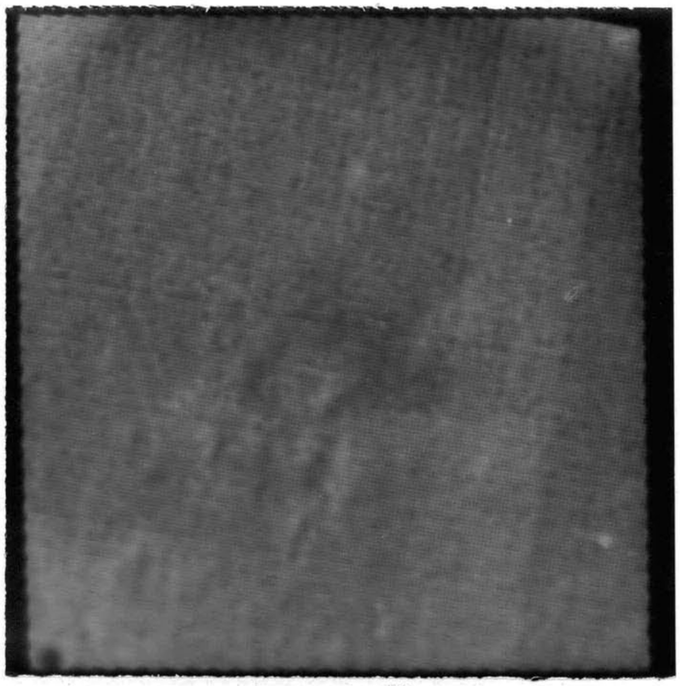

Figure 21a
0.906/0.948 ratio

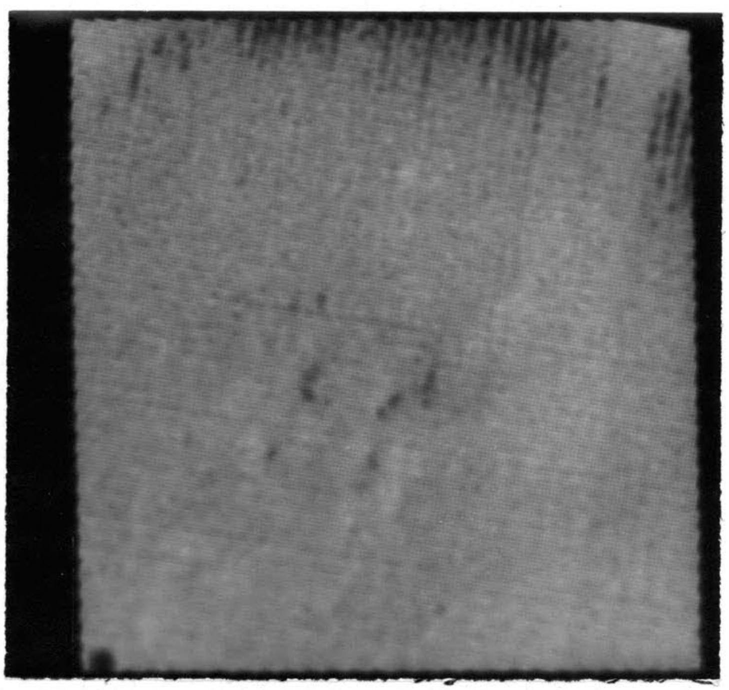

Figure 21b
0.906/0.948 ratio enhanced

Figure 21c

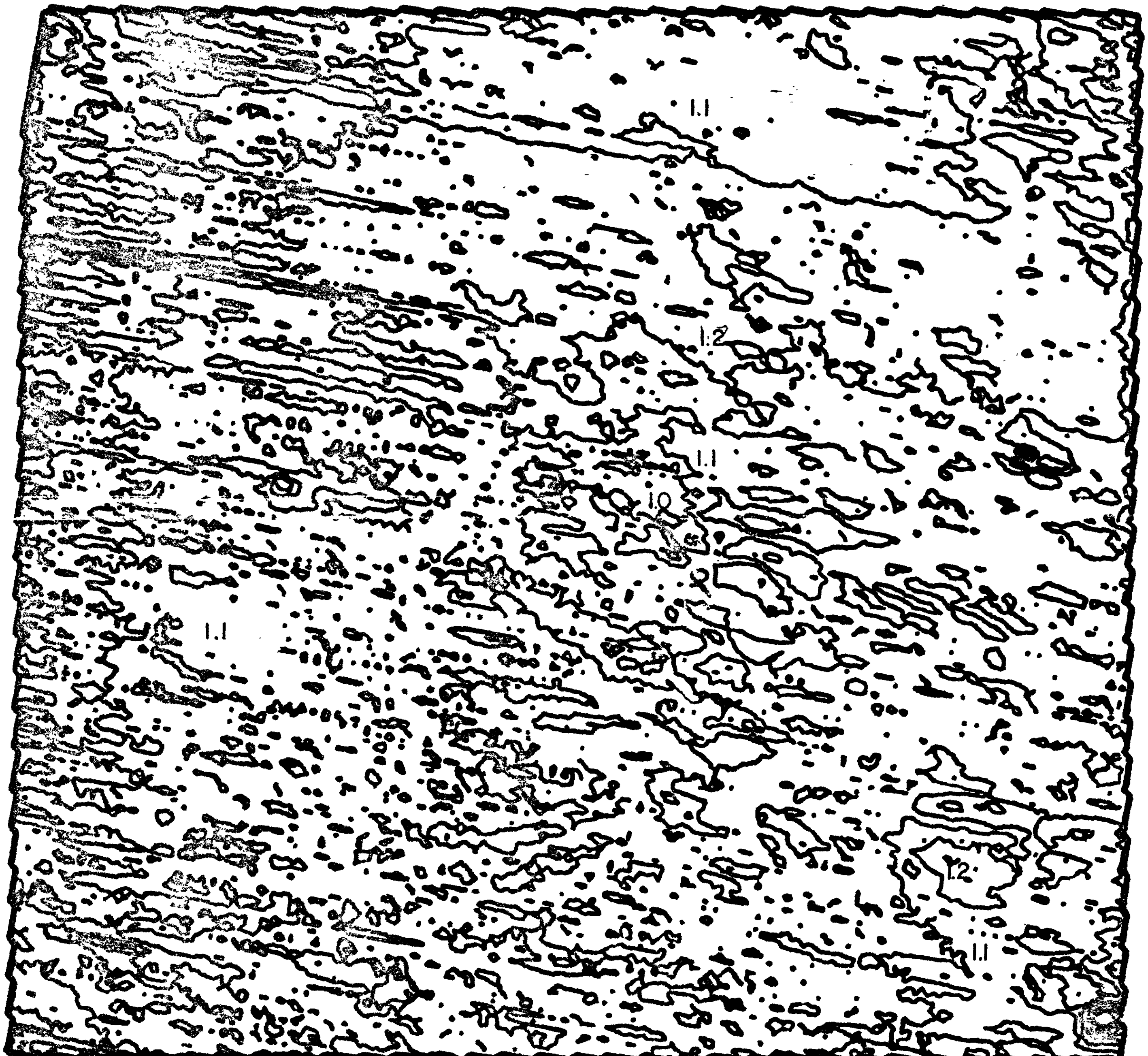

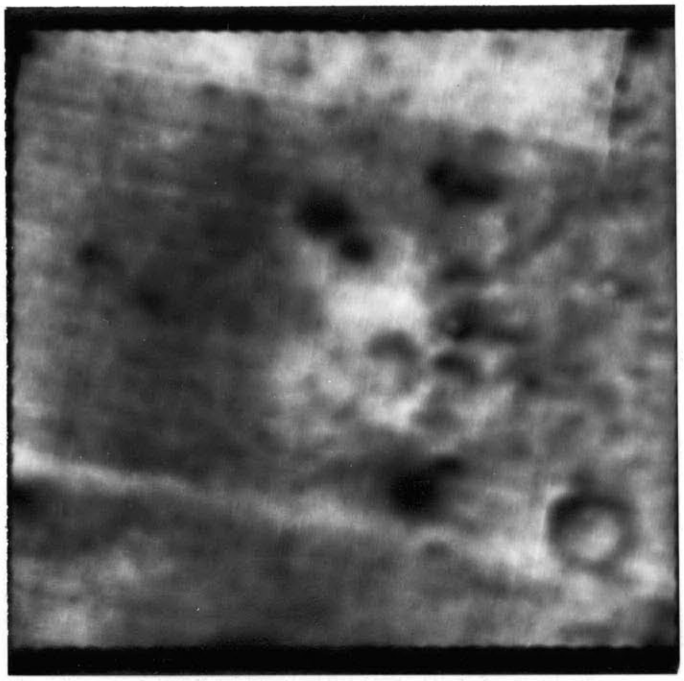

Figure 22a
0.948/0.564 ratio

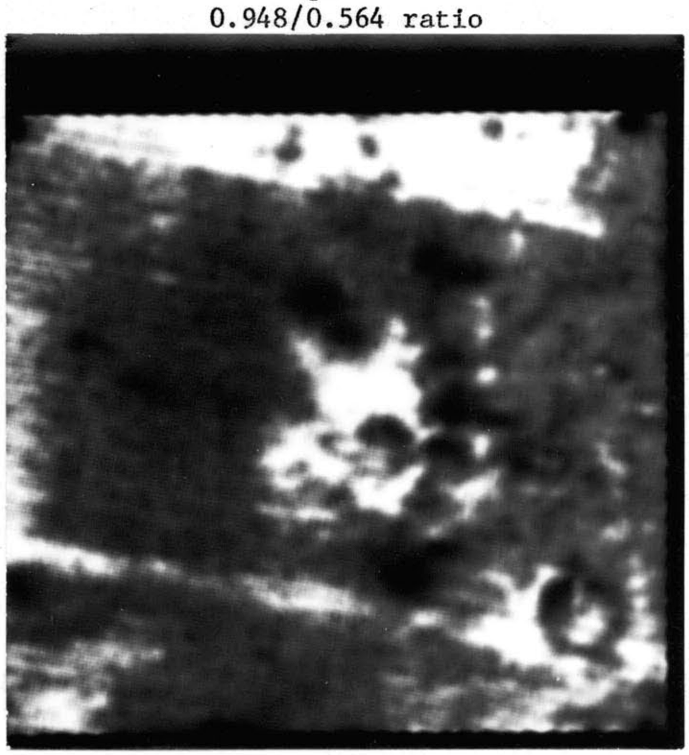

Figure 22b
0.948/0.564 ratio enhanced

Figure 22c

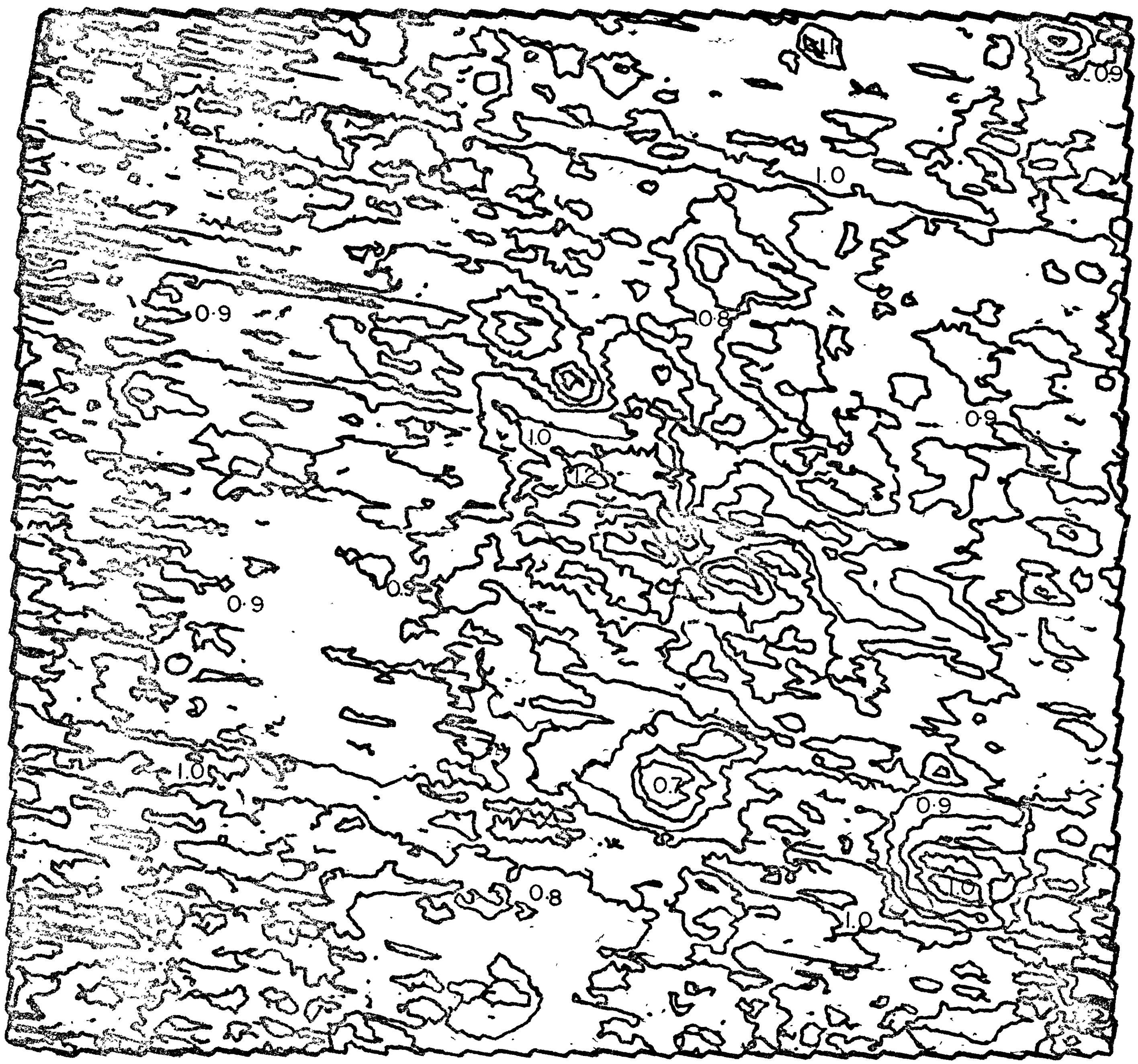

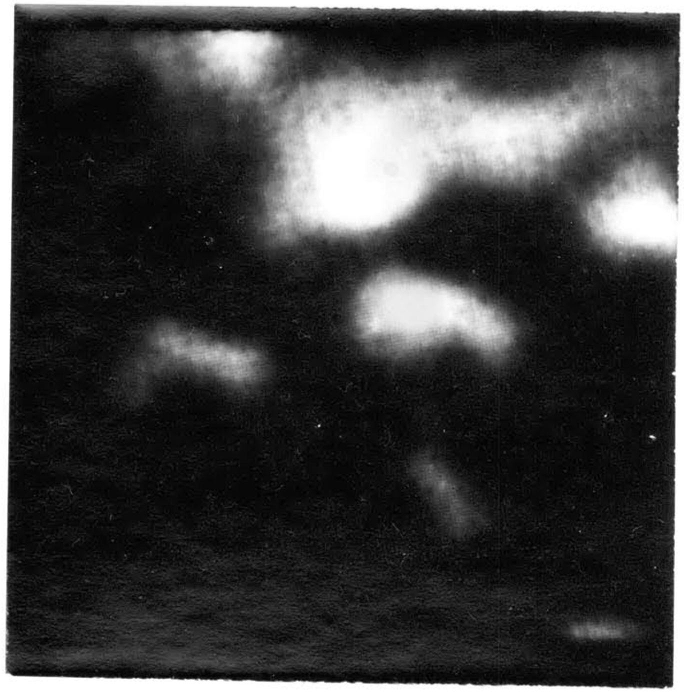

Figure 23
0.402μ, 7 sec exposure

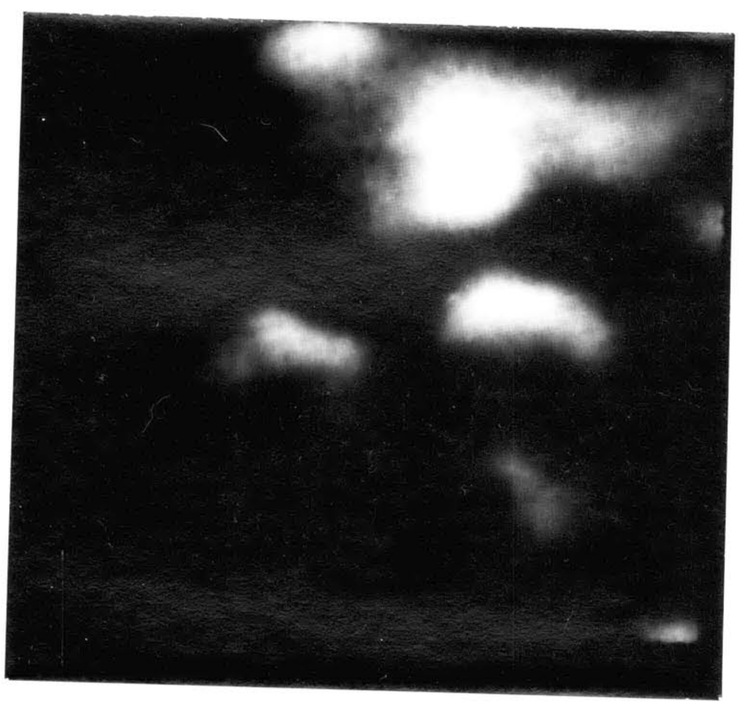

Figure 24
0.564μ, 2 sec exposure

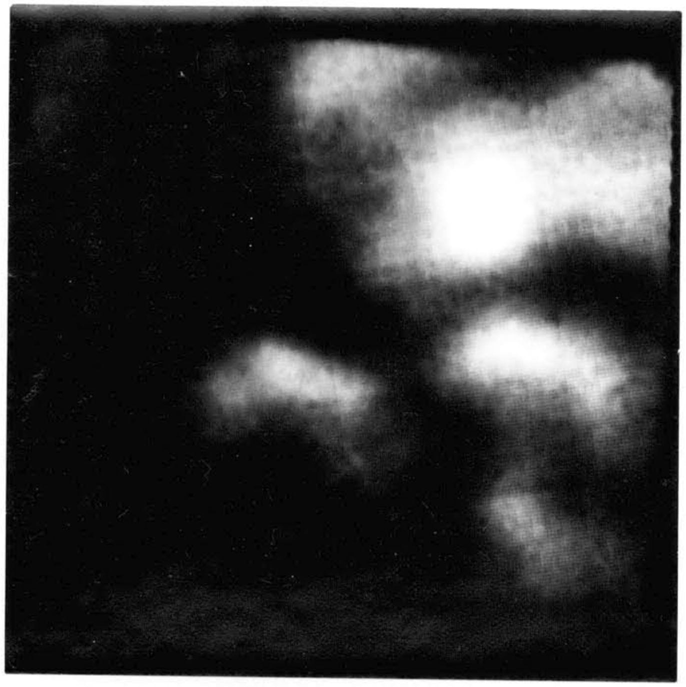

Figure 25
0.906μ, 2.5 sec exposure

Figure 26
0.948μ, 3.5 sec exposure

standard. The 0.906/0.948 ratio again shows a cancellation generally within ±10%.

In order to determine the accuracy to be inferred from the data, a second pair of Cassegrain pictures was used as a check (fig. 30). The ratio of these pictures, 0.402/0.906, is shown in fig. 31. Although the 1.0 level is offset from that in the first ratio in fig. 20, the large-scale features are visible in both. Fig. 32 is the ratio of the two 0.906μ pictures. Although most of the parts fall within a range of ±10%, there is a great deal of scattering within that range. In addition, while the picture is generally featureless, a few areas show low-contrast features. Finally, both 0.402/0.906 ratios are themselves divided in fig. 33. In this ratio, the points are again generally scattered within a ±10% range. It is clear in all of these pictures that the agreement is not perfect, yet the features are repeatable; in particular, there seems to be little or no indication of a systematic error in the ratios.

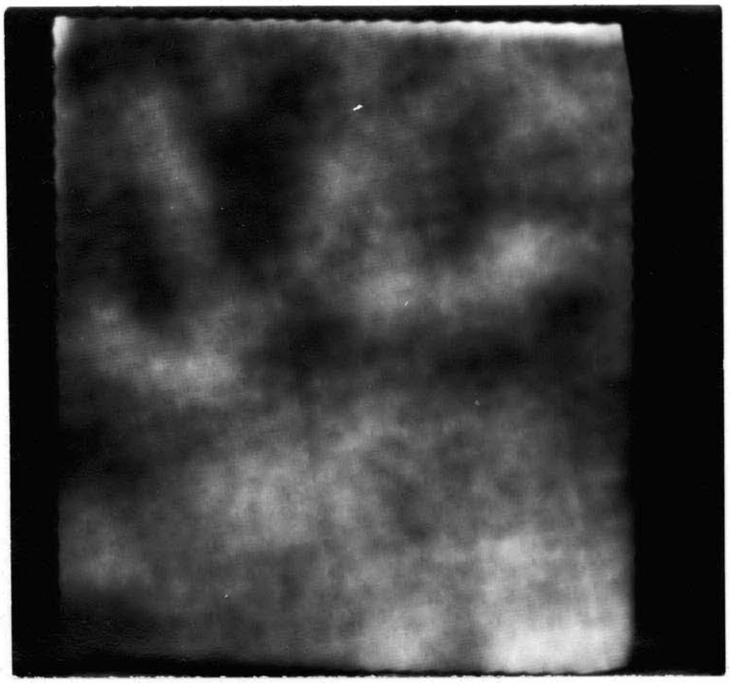

Figure 27a
0.402/0.906 ratio

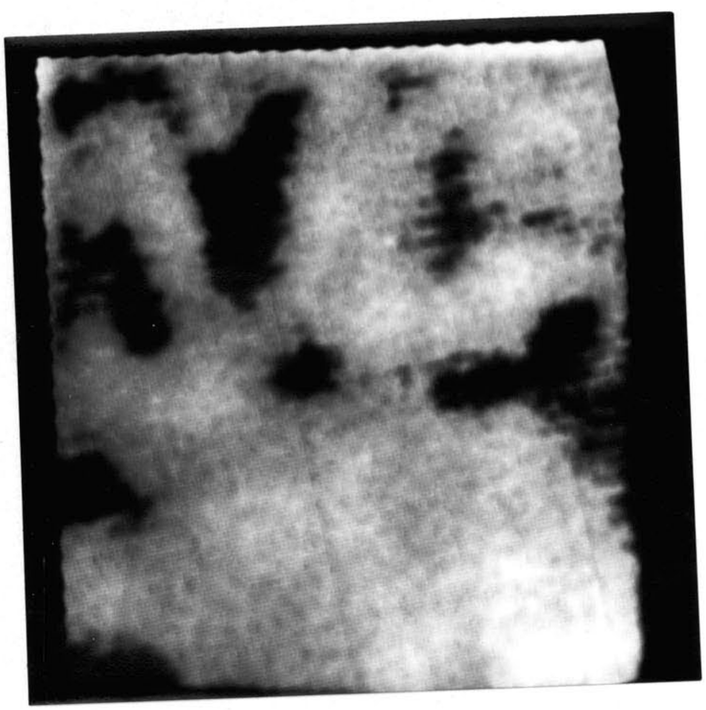

Figure 27b
0.402/0.906 ratio enhanced

Figure 27c

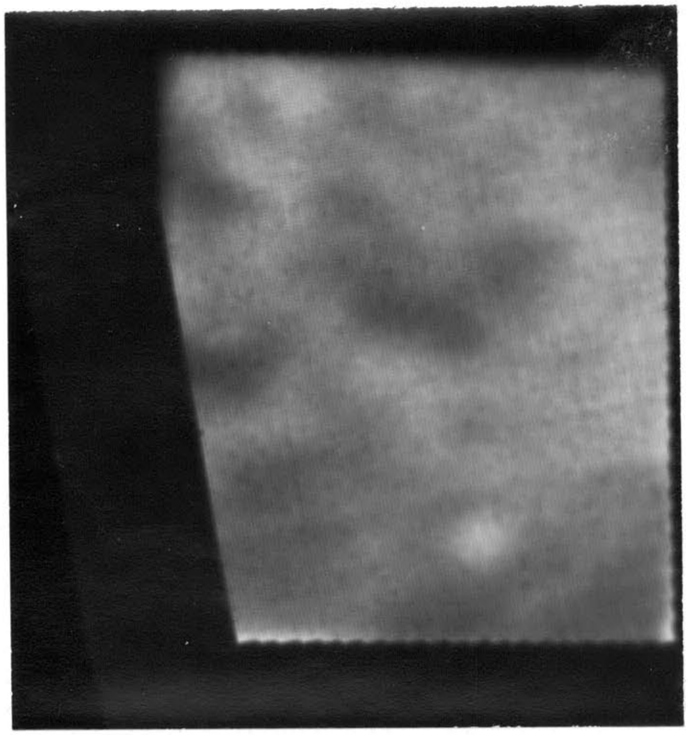

Figure 28a
0.948/0.564 ratio

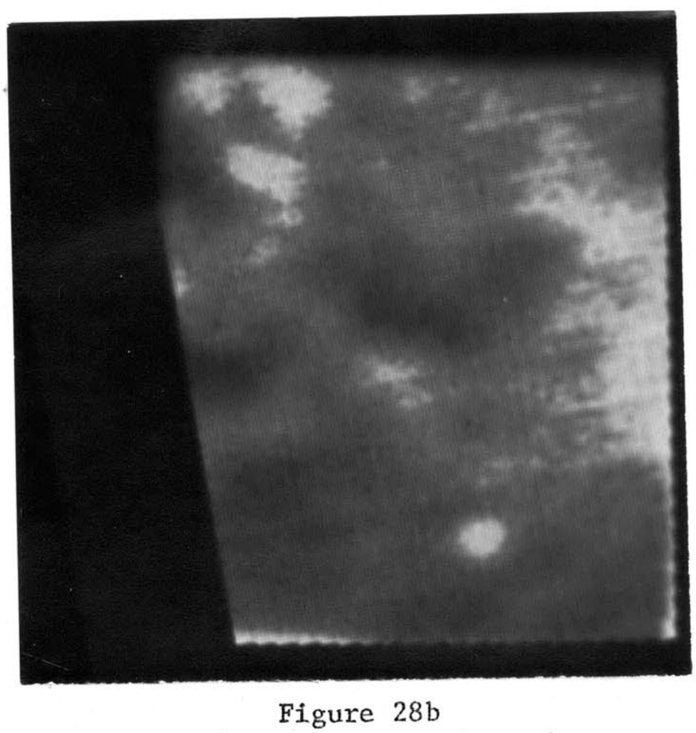

Figure 28b
0.948/0.564 ratio enhanced

Figure 28c

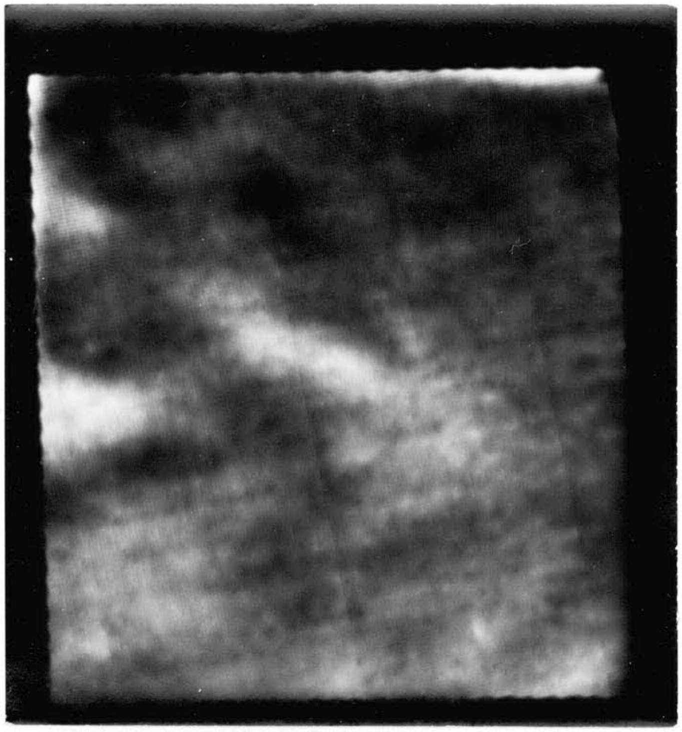

Figure 29a
0.906/0.948 ratio

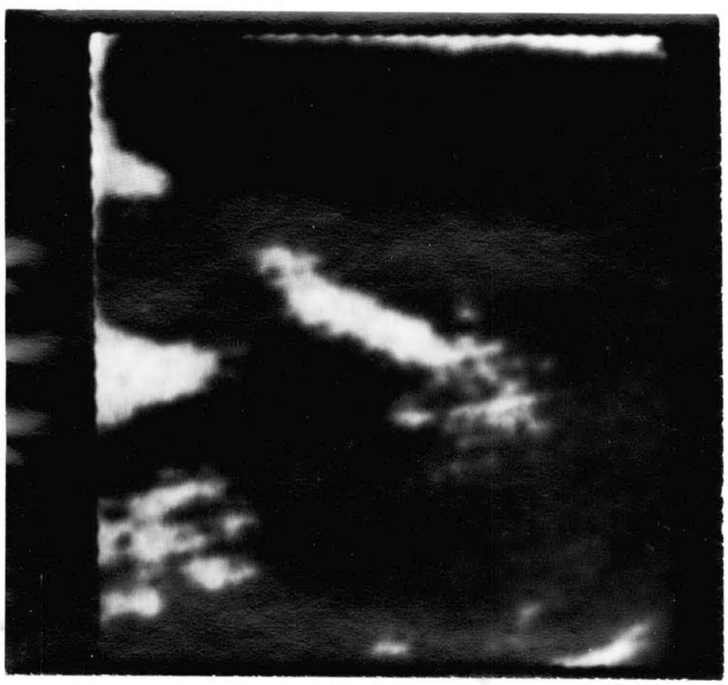

Figure 29b
0.906/0.948 ratio enhanced

Figure 29c

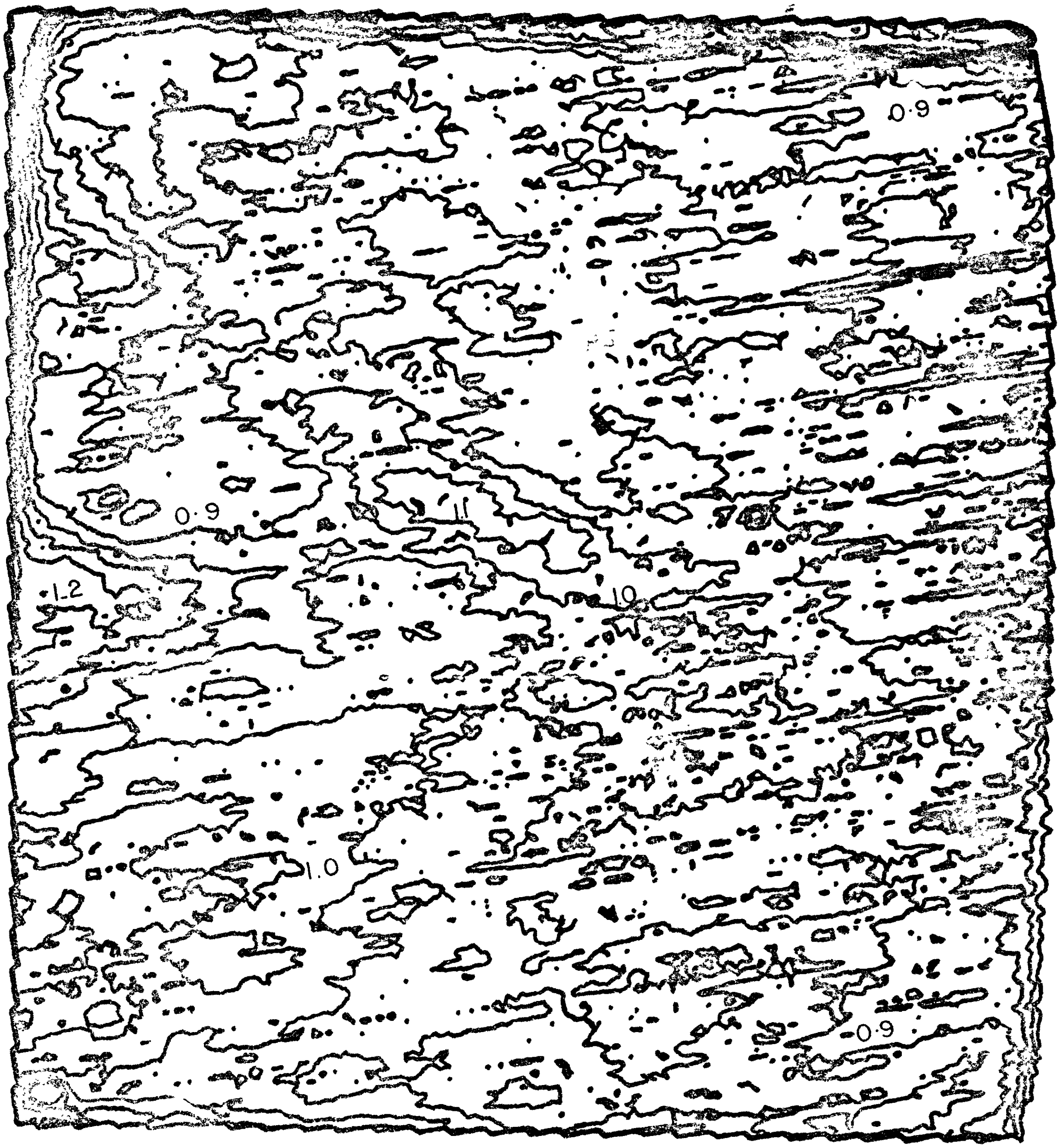

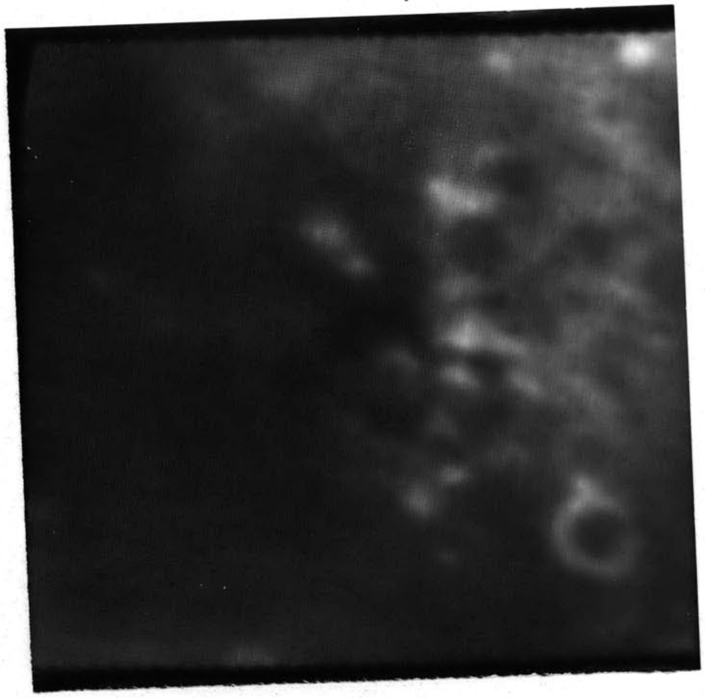

Figure 30a
0.402μ, 0.22 sec exposure

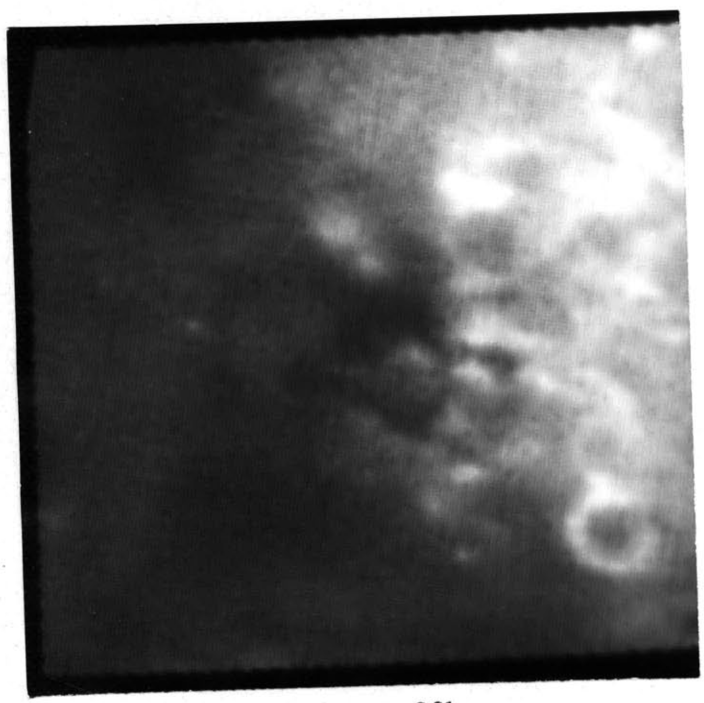

Figure 30b
0.906μ, 0.12 sec exposure

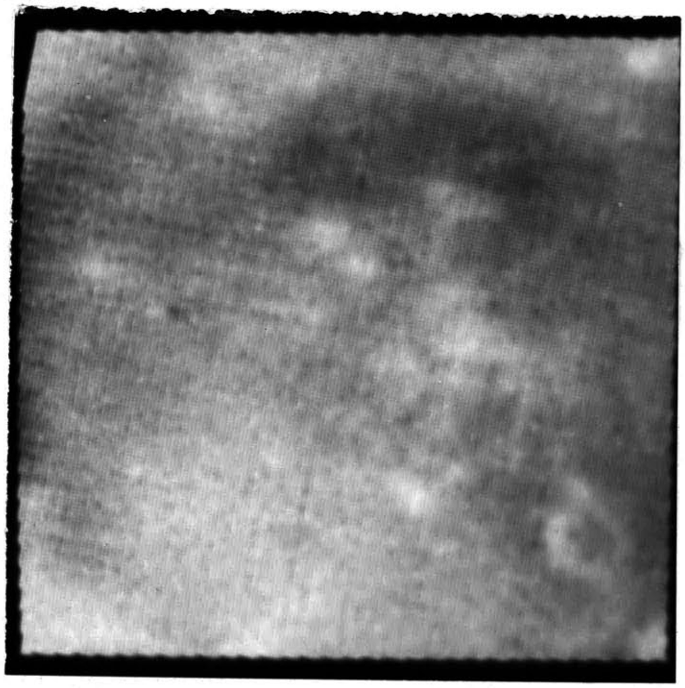

Figure 31a
0.402/0.906 ratio

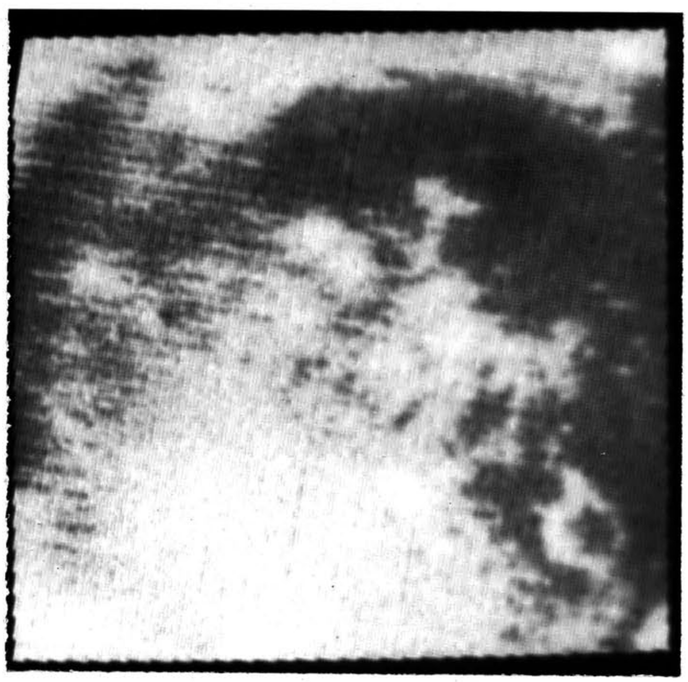

Figure 31b
0.402/0.906 ratio enhanced

Figure 31c

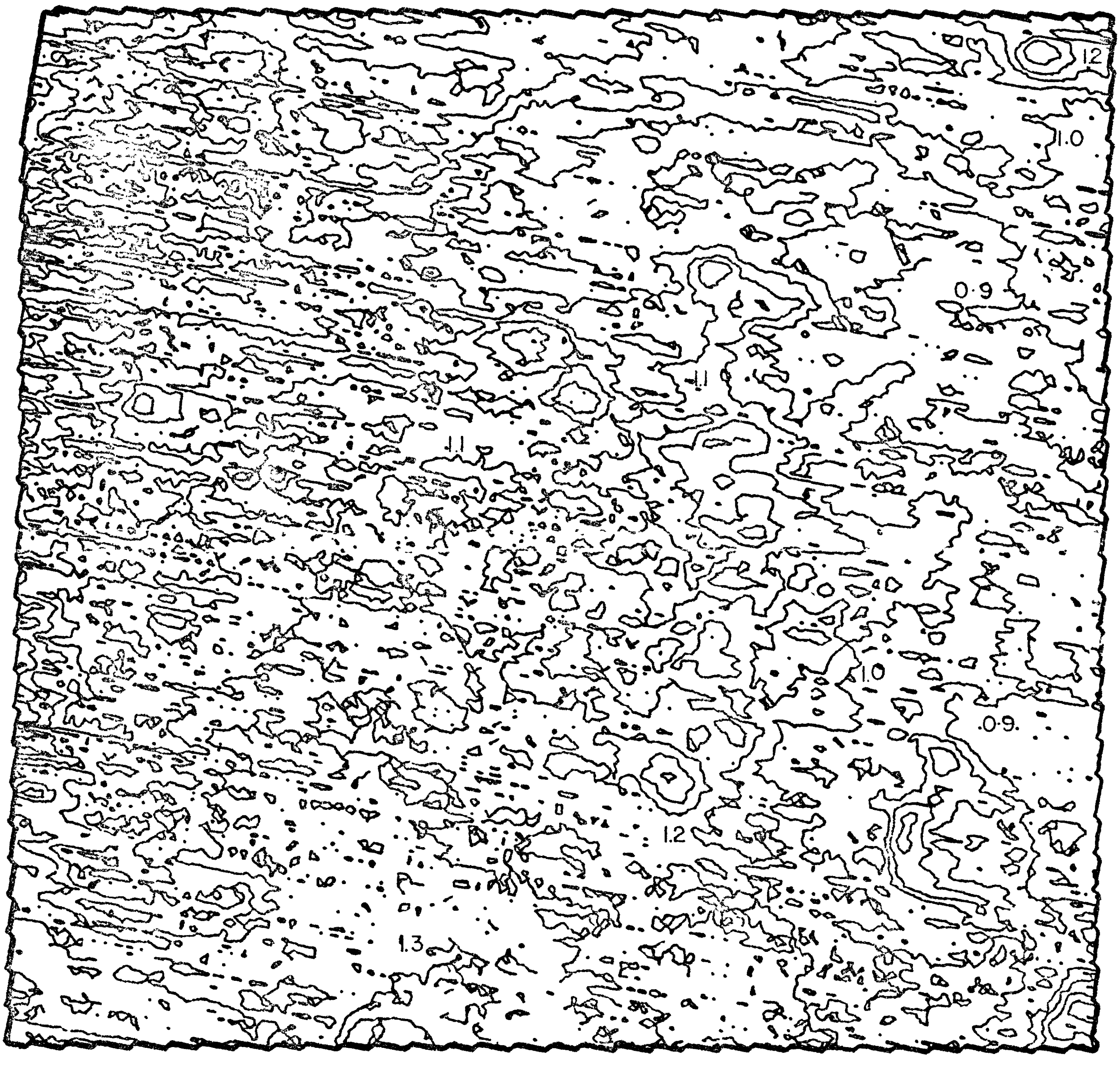

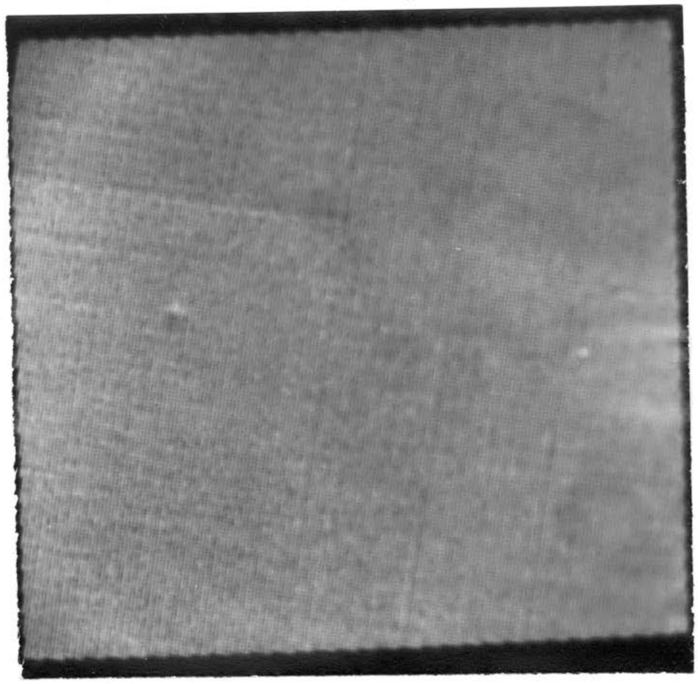

Figure 32a
0.906/0.906 ratio

Figure 32b
0.906/0.906 ratio enhanced

Figure 32c

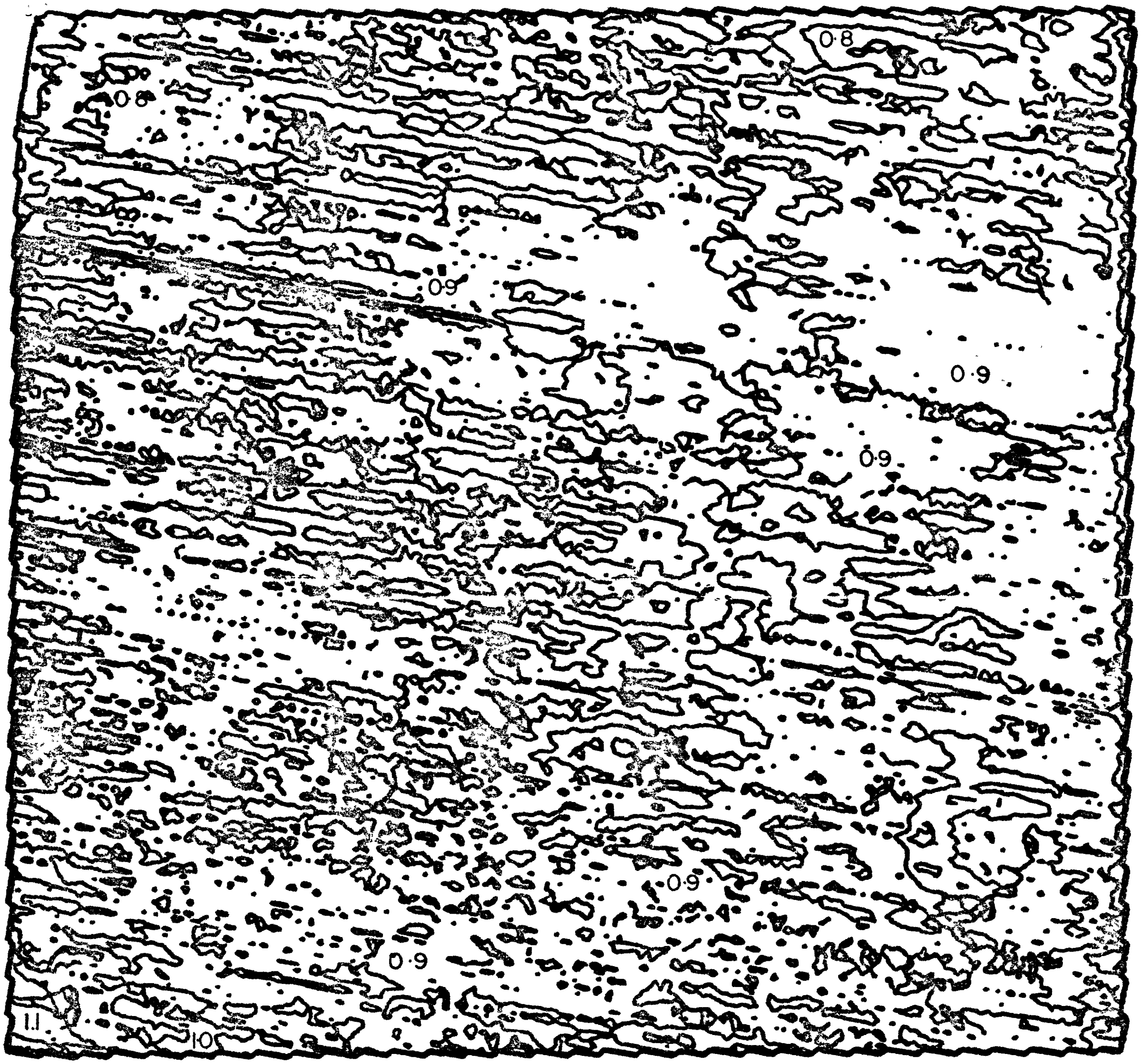

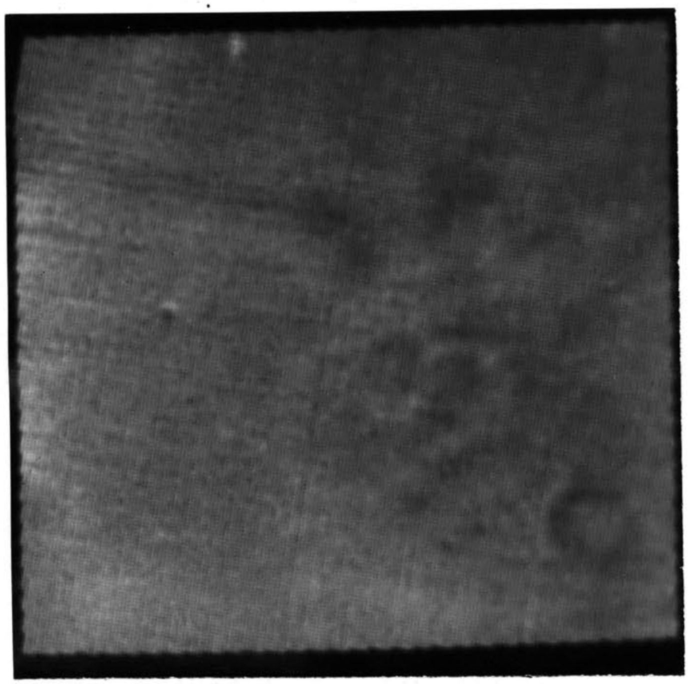

Figure 33a
(0.402/0.906)/(0.402/0.906) ratio

Figure 33b
(0.402/0.906)/(0.402/0.906) ratio enhanced

Figure 33c

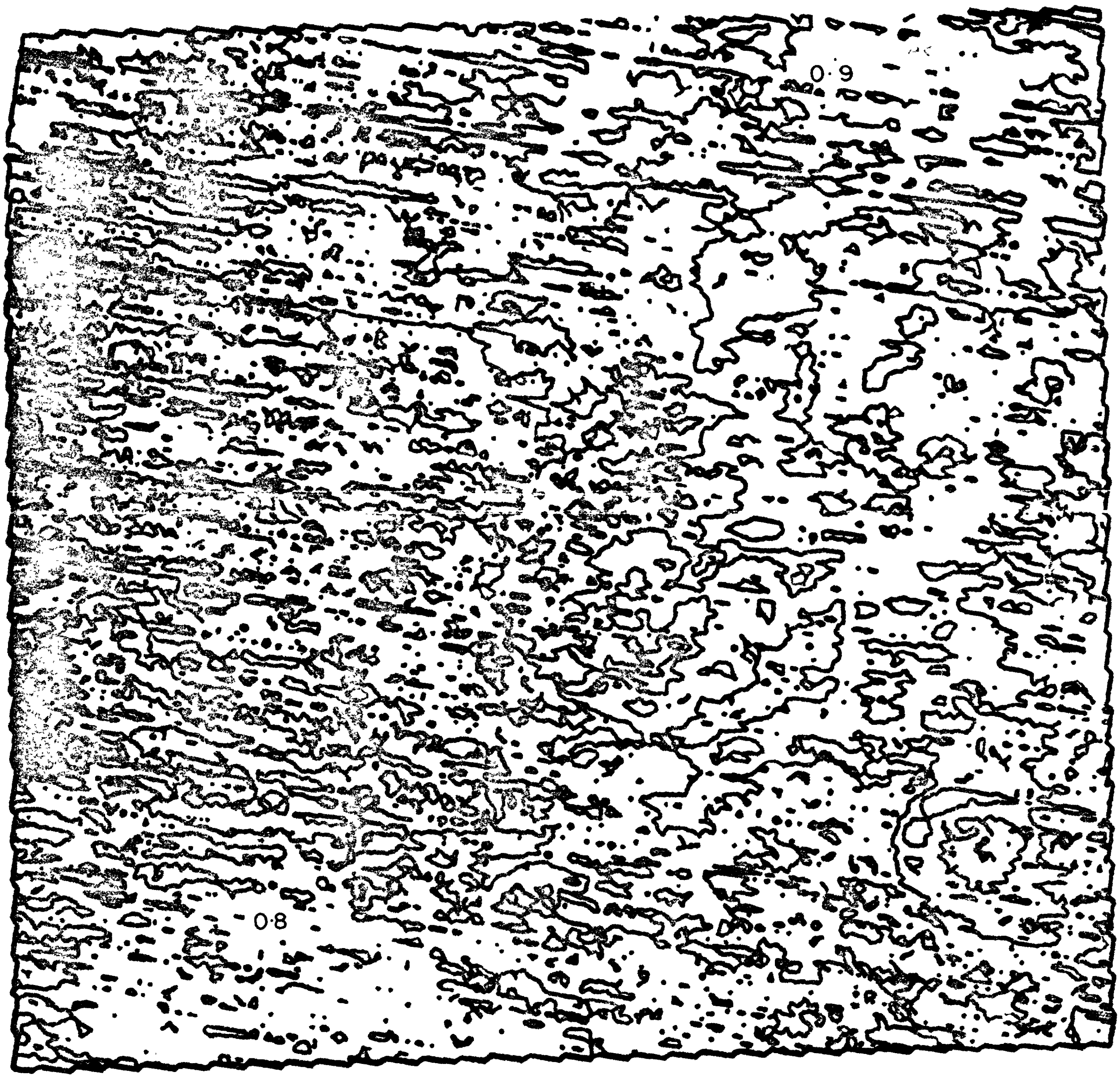

Chapter V -- Conclusions

The pictures displayed in Chapter IV provide an example of the type of results that can be obtained with the vidicon photometer. The developments made in the hardware and software for this project have enabled a complete, if small, observing program to be carried out and run through the system. From the results thus obtained, further improvements can be made, and more data processed. This sequence can be continued indefinitely, but at some point the system should start to produce useful data. It is clear that this vidicon system is capable of doing so, although not at the precision ultimately attainable. Nevertheless, the technique presented here works well enough to make useful contributions to lunar spectral reflectivity work, as well as many other investigations.

Based primarily upon the data presented in this project, modifications to the hardware and observing procedures can be and are being made. Although the full explanation for the failure of pictures to repeat exactly is unknown, several problems have been diagnosed. The major problem in this data appears to be due to the incomplete erasure of the vidicon tube target before exposing the next image. Since the first scan of the target, which is recorded as the data frame, replaces only about 70-80% of the charge across the diodes, several more scans are necessary to ensure that the diodes are completely recharged prior to exposure. However, subsequent scans have less effect on the target charge than would be expected; the effect is also variable across the target and does not correlate well with any observed function. This is undoubtedly the major cause of the occasional large discrepancies in pictures that should match; additionally, it could cause smaller differences across a larger area. Since these data were taken, it has been found that priming the target by completely discharging the diodes before erasing results in a much more uniform erasure. Thus this effect, which in some cases is 10-15%, should be eliminated in future data. This would result in much better repeatability of results, and would bring the quantitative color differences obtained by this project closer to agreement with known data.

A second problem that has been observed is instability in the hardware. The problem with the preamplifier bias drift has been discussed, along with its temporary solution; a new design is expected to provide a more permanent cure. A more subtle effect is due primarily to the manner in which the tube is cooled. The dry ice is necessary to reduce the target temperature below the point where dark current is significant; at the same time, however, the focus and deflection coils, which physically surround the tube, carry constant and varying currents. Thus the coils tend to heat the cold box, and ice must be replaced considerably more often than is normal with a photomultiplier tube. This thermal instability, coupled with a longer-term instability in the high-power deflection amplifiers in the electronics rack, gives rise to a variation in the sampling raster itself. That is, the sampel in the data at a given set of matrix coordinates does not always correspond to the same physical point on the tube target, and therefore on the focal plane. Such raster shifts are nonlinear and can give rise to "ghost" images when two pictures of the same image are divided. This instability can be greatly reduced by a more careful control of the temperature; a better cold box is currently being designed.

The problems discussed above indicate that the vidicon photometry system is still very much in the developmental stage. Nevertheless, usable data is obtainable and the technique seems to be sound. Using the knowledge and experience gained from this project, further improvements have been made on the system. The major causes for the large discrepancies in the data have been found and are being corrected; more flexible data processing procedures are being developed; observing techniques are being made more efficient. The result should be a very powerful tool for accurate two-dimensional photoelectronic imagery.

REFERENCES

Adams, J. B. and T. B. McCord (1970). Remote sensing of lunar surface mineralogy: Implications from visible and near-infrared reflectivity of Apollo 11 samples. Geochim. Cosmochim. Acta, Suppl. 1, 1937-1945.

Adams, J. B. and T. B. McCord (1971). Alteration of lunar optical properties: age and composition effects. Science 171, 567-571.

Crowell, M. H. and E. F. Labuda (1971). In Photoelectronic Imaging Devices, (L. M. Biberman and S. Nudelman, eds.), Vol. 2. Plenum, New York.

Goetz, A. F. H., F. C. Billingsley, J. W. Head, T. B. McCord, and E. Yost (1971). Apollo 12 multispectral photography experiment. In Proceedings of the Second Lunar Science Conference, Vol. 3, M.I.T. Press, Cambridge.

McCord, T. B. (1968). Color differences on the lunar surface. Ph.D. dissertation, California Institute of Technology, Pasadena, California.

McCord, T. B. and J. A. Westphal (1972a). A Silicon Vidicon Photometer. Pub. Astron. Soc. Pacific 84, 133.

McCord, T. B. and J. A. Westphal (1972b). Two-dimensional Silicon Vidicon Astronomical Photometer. Appl. Opt. 11, 522-526.

McCord, T. B., M. P. Charette, T. V. Johnson, L. A. Lebofsky, C. Pieters and J. B. Adams (1972). Lunar Spectral Types. J. G. R. 77, 1349-1359.

Soderblom, L. A. (1970). The distribution and ages of regional lithologies in the lunar maria. Ph.D. dissertation, California Institute of Technology, Pasadena, California.